AD750292

Semi-Annual Technical Report No. 5

(for period Feb. 1, 1972 to July 31, 1972)

Title: Steerable Volume and Surface Spin Waves in Ferrimagnetic Films

Contract No.: DAHC 15 70 C 0190
ARPA Order No.: 1512
Program Code No.: D10

Name of Contractor: Massachusetts Institute of Technology
Cambridge, Massachusetts 02139

Principal Investigator: F. R. Morgenthaler
(617) 253-4623

Effective Date of Contract: Feb. 2, 1970
Contract Expiration Date: Feb. 1, 1973

D D C
RECEIVED
OCT 25 1972
B

Reproduced by
NATIONAL TECHNICAL
INFORMATION SERVICE
U S Department of Commerce
Springfield VA 22151

Sponsored by
Advanced Research Projects Agency
ARPA Order No. 1512

DISCLAIMER NOTICE

THIS DOCUMENT IS THE BEST QUALITY AVAILABLE.

COPY FURNISHED CONTAINED A SIGNIFICANT NUMBER OF PAGES WHICH DO NOT REPRODUCE LEGIBLY.

ACCESSION for
NTIS White Section
DDC Buff Section
UNANNOUNCED
JUSTIFICATION
per previous rpt.
BY
DISTRIBUTION/AVAILABILITY CODES
Dist. AVAIL. and/or SPECIAL
A

The work reported in this document was made possible through support extended the Massachusetts Institute of Technology by the Advanced Research Projects Agency.

Unclassified
Security Classification

DOCUMENT CONTROL DATA - R&D

(Security classification of title, body of abstract and indexing annotation must be entered when the overall report is classified)

1. ORIGINATING ACTIVITY (Corporate author) Massachusetts Institute of Technology, Microwave & Quantum Magnetics Group/ Crystal Physics Laboratory, Dept. of Elec. Engineering and Ctr. for Materials Science and Engrg. Cambridge, Mass. 02139

2a. REPORT SECURITY CLASSIFICATION
Unclassified

2b. GROUP

3. REPORT TITLE

Steerable Volume and Surface Spin Waves in Ferrimagnetic Films

4. DESCRIPTIVE NOTES (Type of report and inclusive dates)
Semi-Annual Technical Report No. 5 Feb. 1, 1972 to July 31, 1972

5. AUTHOR(S) (Last name, first name, initial)

Morgenthaler, Frederic R.

6. REPORT DATE
September 1, 1972

7a. TOTAL NO. OF PAGES

7b. NO. OF REFS

8a. CONTRACT OR GRANT NO.
DARC 15 70 C 0190

b. PROJECT NO.

c.

d.

9a. ORIGINATOR'S REPORT NUMBER(S)
Semi-Annual Technical Report No. 5

9b. OTHER REPORT NO(S) (Any other numbers that may be assigned this report)

10. AVAILABILITY/LIMITATION NOTICES

11. SUPPLEMENTARY NOTES

12. SPONSORING MILITARY ACTIVITY
Advanced Research Projects Agency
Arlington, Virginia 22209

13. ABSTRACT

Magnetostatic modes of resonance were studied in a rectangular slab (.191" long, .162" wide, .018" deep) of single-crystal yttrium iron garnet (YIG). Two moveable fine-wire transducers on opposite faces of the normally-magnetized slab allowed excitation and detection of spatially localized resonances at S-band frequencies. The strength of the detected signal was found to be dependent on the lateral displacement of the sample relative to the transducers. Multiple transmission peaks (corresponding to multiple modes of resonance) exhibited symmetry about the middle of the crystal. The distance of these peaks from the middle of the crystal increased as the excitation frequency was increased, or as the magnetic field was decreased.

It is hypothesized that non-uniform internal magnetic fields, due to the non-ellipsoidal geometry of the sample, are responsible for this phenomenon. The high degree of localization (most resonances were confined to less than one-tenth of the length of the crystal) is attributed to the narrow linewidth of the single crystal (approximately ten oersteds for the lower-order modes) and to the large gradients of internal magnetic field near the edge of the crystal (approximately 2000 oersteds/inch halfway between the center of the crystal and its edge).

The internal magnetic field of the sample is plotted experimentally. The results are shown to be in close agreement with theoretical expectations.

DD FORM 1 JAN 64 1473

Unclassified
Security Classification

14. KEY WORDS	LINK A ROLE	LINK A WT	LINK B ROLE	LINK B WT	LINK C ROLE	LINK C WT
spin waves						
ferrimagnets						
microwaves						
yttrium iron garnet (YIG)						
chemical vapor deposition						
top seeded solution growth						
crystals						
thin films						
magnons magnetostatic						

INSTRUCTIONS

1. ORIGINATING ACTIVITY: Enter the name and address of the contractor, subcontractor, grantee, Department of Defense activity or other organization *(corporate author)* issuing the report.

2a. REPORT SECURITY CLASSIFICATION: Enter the overall security classification of the report. Indicate whether "Restricted Data" is included. Marking is to be in accordance with appropriate security regulations.

2b. GROUP: Automatic downgrading is specified in DoD Directive 5200.10 and Armed Forces Industrial Manual. Enter the group number. Also, when applicable, show that optional markings have been used for Group 3 and Group 4 as authorized.

3. REPORT TITLE: Enter the complete report title in all capital letters. Titles in all cases should be unclassified. If a meaningful title cannot be selected without classification, show title classification in all capitals in parenthesis immediately following the title.

4. DESCRIPTIVE NOTES: If appropriate, enter the type of report, e.g., interim, progress, summary, annual, or final. Give the inclusive dates when a specific reporting period is covered.

5. AUTHOR(S): Enter the name(s) of author(s) as shown on or in the report. Enter last name, first name, middle initial. If military, show rank and branch of service. The name of the principal author is an absolute minimum requirement.

6. REPORT DATE: Enter the date of the report as day, month, year; or month, year. If more than one date appears on the report, use date of publication.

7a. TOTAL NUMBER OF PAGES: The total page count should follow normal pagination procedures, i.e., enter the number of pages containing information.

7b. NUMBER OF REFERENCES: Enter the total number of references cited in the report.

8a. CONTRACT OR GRANT NUMBER: If appropriate, enter the applicable number of the contract or grant under which the report was written.

8b, 8c, & 8d. PROJECT NUMBER: Enter the appropriate military department identification, such as project number, subproject number, system numbers, task number, etc.

9a. ORIGINATOR'S REPORT NUMBER(S): Enter the official report number by which the document will be identified and controlled by the originating activity. This number must be unique to this report.

9b. OTHER REPORT NUMBER(S): If the report has been assigned any other report numbers *(either by the originator or by the sponsor)*, also enter this number(s).

10. AVAILABILITY/LIMITATION NOTICES: Enter any limitations on further dissemination of the report, other than those imposed by security classification, using standard statements such as:

(1) "Qualified requesters may obtain copies of this report from DDC."

(2) "Foreign announcement and dissemination of this report by DDC is not authorized."

(3) "U. S. Government agencies may obtain copies of this report directly from DDC. Other qualified DDC users shall request through _____."

(4) "U. S. military agencies may obtain copies of this report directly from DDC. Other qualified users shall request through _____."

(5) "All distribution of this report is controlled. Qualified DDC users shall request through _____."

If the report has been furnished to the Office of Technical Services, Department of Commerce, for sale to the public, indicate this fact and enter the price, if known.

11. SUPPLEMENTARY NOTES: Use for additional explanatory notes.

12. SPONSORING MILITARY ACTIVITY: Enter the name of the departmental project office or laboratory sponsoring *(paying for)* the research and development. Include address.

13. ABSTRACT: Enter an abstract giving a brief and factual summary of the document indicative of the report, even though it may also appear elsewhere in the body of the technical report. If additional space is required, a continuation sheet shall be attached.

It is highly desirable that the abstract of classified reports be unclassified. Each paragraph of the abstract shall end with an indication of the military security classification of the information in the paragraph, represented as *(TS)*, *(S)*, *(C)*, or *(U)*.

There is no limitation on the length of the abstract. However, the suggested length is from 150 to 225 words.

14. KEY WORDS: Key words are technically meaningful terms or short phrases that characterize a report and may be used as index entries for cataloging the report. Key words must be selected so that no security classification is required. Identifiers, such as equipment model designation, trade name, military project code name, geographic location, may be used as key words but will be followed by an indication of technical context. The assignment of links, rules, and weights is optional.

GPO 886-551

Unclassified
Security Classification

ABSTRACT (Continued)

The actual path taken by the wave energy through the crystal is quite complex, because the direction of power flow is in general not parallel to the wave vector, but is inclined at an angle (the beam steering angle) that is dependent on the angle between the d.c. magnetization and the propagation vector. Such considerations are reviewed theoretically because of their possible importance in interpretingthe thesis results.

PREFACE

The Microwave and Quantum Magnetics Group and the Crystal Physics Laboratory, both within the M.I.T. Center for Materials Science and Engineering, have undertaken a three year interdisciplinary program in the area of "microwave magneto-ultrasonics" aimed at further developing several novel concepts which may lead to new and/or improved solid state devices employing electromagnetic/spin/elastic wave coupling. Device possibilities include multi-tapped delay lines, magnetoelastic beam switches and pulse compression filters. In particular, the research program will concentrate on the growth and exploitation of improved single crystal yttrium iron garnet substrates in which volume and surface spin wave propagating at microwave frequencies can be magnetically steered and/or otherwise controlled.

In order to produce crystals of yttrium iron garnet of the quality needed for the research envisioned in this program, two major constraints must be dealt with. First, the crystals must be of the necessary high quality to avoid introducing extraneous effects due to grain boundaries and strain inhomogeneities. The chemical purity is of major importance since rare earth impurities drastically increase spin wave relaxation rates. Second, the growth technique should permit ready fabrication of the types of structures desired, such as multi-layer configurations and thin slabs. Consequently,

both chemical vapor deposition (CVD) techniques and top-seeded solution (TSS) growth appear attractive and both will be employed throughout the entire contract period. Thin films and bulk crystal substrates will be evaluated optically, magnetically and acoustically for purity, homogeneity and low losses. Promising specimens will be used for magnetostatic wave and exchange dominated spin wave propagation experiments at microwave frequencies.

A surface spin wave propagating parallel to an air-crystal boundary of a thin film has its energy largely confined within some characteristic distance that under certain conditions should be magnetically controllable. In one instance causing the energy to be closely confined to the surface and in another allowing it to spread out and fill the entire film. Volume spin waves are also subject to magnetic control. For example, beam steering is possible due to dipole-dipole interactions that in turn can be influenced through directional changes in the magnetizing field.

Dr. A. Linz has been assigned responsibility for overseeing the top-seeded solution crystal growth and chemical vapor deposition program, Professor D. J. Epstein for crystal evaluation with respect to magnetic properties and Professor F. R. Morgenthaler for microwave spin wave propagation studies; as principal investigator the latter has overall responsibility for coordinating the various phases of the research.

This report is based upon material contained in the S.M. Thesis of Carl Frederic Olenberger III to be submitted to the M.I.T. Department of Electrical Engineering. The research reports our preliminary work on Localized Resonance in Single Crystal Yttrium Iron Garnet.

SECTION 1.0 Introduction

The gyromagnetic nature of ferrite materials has led to a large class of microwave devices such as isolators, Faraday rotators, and circulators. Their operation is conveniently analyzed and understood in terms of wave propagation in a medium characterized by a tensor permeability. The electromagnetic radiation couples with the spin system of the ferrite at low values of wave number $k(1/10 - 1cm^{-1})$.

More recently, advances in crystal growing techniques have resulted in the availability of sizeable high-quality single crystals of materials such as yttrium iron garnet (YIG). With such crystals, it is possible to couple with the spin system at much higher values of k. It can be shown that at higher values of $k(k > 100cm^{-1})$, the energy propagation is sufficiently slow for the magnetostatic approximation to hold. This higher k range of the spin-wave spectrum is therefore known as the magnetostatic region.

Although magnetostatic spin waves have been studied extensively, comparatively little experimental work has dealt with the detailed nature of the energy path of these waves through a crystal. This thesis was initiated in order to provide a better understanding of this subject. In particular, magnetostatic modes of resonance were studied in a small rectangular slab of single-crystal

YIG. Two moveable fine-wire transducers on opposite faces of the normally-magnetized slab allowed excitation and detection of spatially localized resonances at S-band frequencies.

The actual path taken by the wave energy through the crystal is quite complex, because the direction of power flow is in general not parallel to the wave vector, but is inclined at an angle that is dependent on the angle between the d.c. magnetization and the propagation vector. Such considerations are reviewed theoretically because of their possible importance in interpreting the thesis results.

This report is organized as follows:

Starting from Maxwell's equations and an equation of motion which takes into account the effects of exchange, the spin wave dispersion relation is derived in Section 2. A simplified expression is given in the magnetostatic approximation ($k >> k_o$), which leads to a discussion of magnetostatic modes in ellipsoidal samples.

Section 3 is directed specifically to the nature of the energy path of a magnetostatic spin wave through a crystal. Using the theory presented in the first two chapters, and neglecting exchange effects, an expression is derived which relates the direction of power flow in a uniformly magnetized sample to the external angle of the

magnetic field. The sensitivity of the beam steering angle to small changes in the magnetic field angle is emphasized, and possible applications are suggested.

Section 4 describes experimental attempts to observe the beam steering effect described in Chapter II. It is discovered that a non-uniform magnetic field inside the experimental YIG sample gives rise to localized resonances. This phenomenon is found to conceal any effects of beam steering but makes feasible the employment of localized resonances in the design of signal processing devices. The conclusions are summarized in Section 5.

SECTION 2.0

Spin Waves and Magnetostatic Modes

The purpose of this section is to give a phenomenological description of the modes of oscillation of magnetic systems. The phenomenological approach is essentially a classical one in which small oscillations of the magnetization about its equilibrium value are studied, and use is made of the classical equations of motion. An alternative approach would be to study the magnetic system from a microscopic viewpoint, with special attention given to localized spins at assigned lattice sites. This latter approach is quantum-mechanical, and such a treatment may be found in the literature.[4,13]

2.1 Spin Waves[3,5,13]

From a macroscopic standpoint, a ferromagnet may be looked upon as a continuous medium characterized by a magnetic moment density $\bar{M}(\bar{r})$, which in the general case is a vector function of a point $\bar{r}$ in space. We shall consider that when the sample is in a state of magnetic saturation, the state corresponding to the least energy is a state of uniform magnetization distribution such that $\bar{M}(\bar{r})$ is constant in the magnitude and direction over the whole volume of the sample.[3] A spin wave may be defined classically as the propagation of small disturbances of the magnetization vector about the

static equilibrium configuration.[13] The spin wave can propagate by virtue of the exchange field which provides a restoring torque tending to align all magnetic dipoles parallel to one another. The exchange field is quantum-mechanical and has no classical analog, but if the wave length of the disturbance is much greater than the inter-atomic distances of the ferromagnetic substance, we are justified in using the classical approach.

The equation of motion, neglecting damping, for the uniform precessional mode is given by

$$\dot{\bar{M}} = \gamma(\bar{M} \times \bar{H}). \tag{2.1}$$

It has been shown[14] that non-uniform modes of precession may be characterized by the addition of a spin-wave term, which is a function of the magnetization $\bar{M}$ and its Laplacian, the square of the distance between spin-dipoles a, an exchange field H_{ex}, and the gyromagnetic ratio γ. With the addition of this term, the equation of motion becomes

$$\dot{\bar{M}} = \gamma(\bar{M} \times \bar{H}) + \gamma H_{ex}\, a^2 \frac{\bar{M} \times \nabla^2 \bar{M}}{|\bar{M}|} \tag{2.2}$$

We may substitute the expressions for the magnetization and magnetic field, neglecting demagnetizing factors,

$$\bar{M} = M_o\, \hat{i}_z + \bar{m} e^{j(\omega t - \bar{k} \cdot \bar{r})} \tag{2.3}$$

and

$$\bar{H} = H_i \, \hat{i}_z + \bar{h} e^{j(\omega t - \bar{k} \cdot \bar{r})} \tag{2.4}$$

into the equation of motion (2.2). Because of the occurrence of the Laplacian operator, it has become necessary in (2.3) and (2.4) to specify the spatial dependence of the r.f. magnetization and magnetic field.

Substituting (2.3) and (2.4) into (2.2) and solving for the r.f. magnetization, we obtain

$$m_x = \frac{\gamma M (h_x \omega_r - j\omega h_y)}{\omega_r^2 - \omega^2} \tag{2.5}$$

and

$$m_y = \frac{\gamma M (h_y \omega_r + j\omega h_x)}{\omega_r^2 - \omega^2} \tag{2.6}$$

where $\omega_r = \gamma (H_i + H_{ex} a^2 k^2)$. The elements of the susceptibility tensor are,

$$\chi_{xx} = \frac{\omega_m \omega_r}{\omega_r^2 - \omega^2}$$

and (2.7)

$$\chi_{yx} = \frac{j\omega \, \omega_m}{\omega_r^2 - \omega^2}$$

In this discussion damping has been neglected, so that in the above equations there is a singularity when $\omega = \omega_r$; this defines an intrinsic resonance frequency for a spin wave. The actual dispersion relation, however,

must take into account any components of $\bar{h}$ due to the spatial pattern of $\bar{m}$ and $\frac{\partial \bar{e}}{\partial t}$.

In deriving the spin wave dispersion relation, then, we will start with Maxwell's curl equations. Assuming $e^{j\omega t}$ time dependence, these are

$$\nabla \times \bar{e} = -j\omega\bar{\bar{\mu}} \cdot \bar{h} \tag{2.8}$$

and

$$\nabla \times \bar{h} = j\omega\varepsilon\bar{e} \tag{2.9}$$

For the material of interest, the permeability is a tensor, the permitivity is a scaler, and the conductivity is negligible.

These facts are reflected in the way (2.8) and (2.9) are written. Eliminating $\bar{e}$ from (2.8) and (2.9) in the usual fashion,

$$-\nabla^2\bar{h} + \nabla(\nabla \cdot \bar{h}) = \omega^2\varepsilon\bar{\bar{\mu}} \cdot \bar{h}. \tag{2.10}$$

The solution of this equation is of the form $\bar{h} = \bar{h}_o e^{j\bar{k} \cdot \bar{r}}$. Substituting this into (2.10),

$$k^2\bar{h} - \bar{k}(\bar{k} \cdot \bar{h}) = \omega^2\varepsilon\bar{\bar{\mu}} \cdot \bar{h} \tag{2.11}$$

Without loss of generality, we may assume that the magnetic field is in the z-direction, and orient the coordinate system so that the k-vector is in the xz plane. We can then define an angle Ψ between the k-vector and the d.c. magnetic field vector so that the components of the k-vector

can be written

$$k_x = |k| \sin \Psi$$

and (2.12)

$$k_y = |k| \cos \Psi$$

Substituting the expression for the tensor permeability

$$\mu = \mu_o \begin{bmatrix} \mu & -j\kappa & 0 \\ j\kappa & \mu & 0 \\ 0 & 0 & 1 \end{bmatrix} \tag{2.13}$$

and equations (2.12) into (2.11), we arrive at three equations linear in h_x, h_y, and h_z. These are

$$(k^2\cos^2\Psi - k_o^2\mu)h_x + (jk_o^2\kappa)h_y + (-k^2\sin\Psi\cos\Psi)\ h_z = 0 \tag{2.14}$$

$$(-jk_o^2\kappa)h_x + (k^2 - k_o^2\mu)h_y = 0 \tag{2.15}$$

$$(-k^2\sin\Psi\cos\Psi)h_x + (k^2\sin\Psi - k_o^2)\ h_z = 0 \tag{2.16}$$

where $k_o^2 = \omega^2\varepsilon\mu_o$. For a non-trivial solution to this set of equations, the determinant of the coefficients must vanish. Expanding the determinant results in an equation which is biquadratic in k. Thus the solution for k^2 is straightforeward, and the result is

$$\frac{k^2}{k_o^2} = \frac{(\mu^2-\mu-\kappa^2)\ \sin^2\Psi + 2\mu \pm [(\mu^2-\mu-\kappa^2)\ \sin^4\Psi\ + 4\kappa^2\cos^2\Psi]^{1/2}}{2[(\mu - 1)\ \sin^2\Psi + 1]} \tag{2.17}$$

The introduction of the permeability tensor was for convenience. The components of the permeability tensor (2.13) are related to the components of the susceptibility tensor by the expressions

$$\mu = 1 + \chi_{xx}$$

and (2.18)

$$j\kappa = -\chi_{xy},$$

where χ_{xx} and χ_{xy} were derived earlier in this chapter to include the effects of exchange, and are given by equations (2.7). Bearing in mind, then, that κ and μ in (2.17) are functions of ω and k, (2.17) may be solved for ω as a function of k. This has been done in the literature,[5] and the result is shown graphically in Fig. 2.1 for the limiting cases $\Psi = 0$ and $\Psi = \pi/2$.

It is possible to define three regions in Fig. 2.1. In the first region, for small values of k, the dispersion diagram is essentially that of an ordinary dielectric. As k increases beyond the value of the free-space wave number for a given frequency, the curve flattens out. In this second region, r.f. magnetic field propagation and the magnetostatic approximation $\nabla \times \bar{h} = 0$ holds.

As the wave number gets very large, exchange effects become important. Using the approximation $k >> k_o$ in (2.17) and substituting the expressions for μ and κ from (2.18) and (2.7) we obtain a simplified expression for

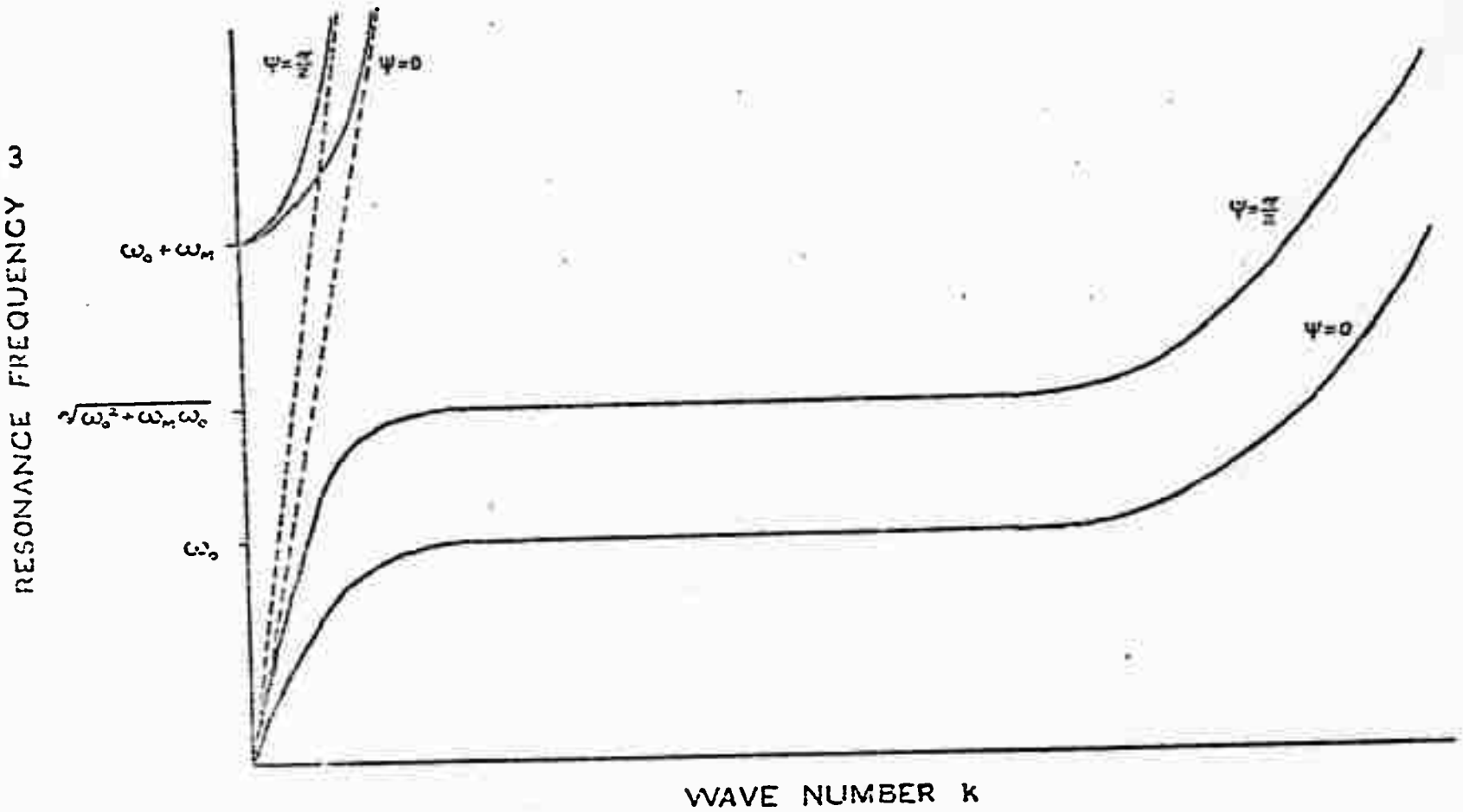

Fig. 2.1 Spin-wave dispersion diagram.

this third region:

$$\omega = [(\omega_o + \omega_{ex}a^2k^2)(\omega_o + \omega_{ex}a^2k^2 + \omega_m \sin^2\Psi)]^{1/2} \qquad (2.19)$$

For the second (magnetostatic) region of the dispersion diagram, the exchange terms in (2.19) may be ignored. The next section will deal specifically with the magnetostatic region of the spectrum.

2.2 Magnetostatic Modes[5,16]

The experimental observation of multiple absorption peaks in ferrimagnetic resonance by White and Solt[15] led to theoretical investigations as to whether samples could oscillate in modes other than that of uniform precession. In their experiment, an inhomogenous r.f. driving field was required to produce the multiple absorptions. The explanation for the appearance of these modes has been given by Walker,[16] and his theory is now widely accepted. The multiple absorption peaks are caused by a variation of phase and amplitude of the r.f. magnetization in different zones within the sample. For this reason, it is also possible to excite these modes (called magnetostatic modes) with an externally uniform driving field if the specimen is finite and non-ellipsoidal, since for such specimens the internal r.f. field will always be non-uniform. For purposes of analysis and classification of the modes, however, it is best to consider ellipsoids and their various degenerate forms, excited by an inhomogenous driving field; otherwise, the non-uniform d.c.

magnetic field within the sample makes the analysis very difficult. Furthermore, a reasonable solution requires that the magnetic field direction be along an axis of the ellipsoid. Thus in the analysis which follows, we will consider a spheroid placed in a magnetic field which points along its symmetry axis. The internal d.c. field is $\bar{H}_i = \bar{H}_o - N_z\, 4\pi\bar{M}_o$. We may solve for the linearized components of the r.f. magnetization in terms of the r.f. magnetic field and the appropriate components of the susceptibility tensor. The resulting expressions will take the form

$$4\pi m_x = \chi_{xx}\, h_x + \chi_{xy}\, h_y$$

and (2.20)

$$4\pi m_y = \chi_{yx}\, h_x + \chi_{yy} h_y$$

The magnetostatic approximation $\nabla \times \bar{h} = 0$ implies that the r.f. magnetic field can be expressed as the gradient of a scaler magnetic potential Ψ. Therefore, (2.20) can be written

$$4\pi m_x = \chi_{xx} \frac{\partial \Psi}{\partial x} + \chi_{xy} \frac{\partial \Psi}{\partial y}$$

and (2.21)

$$4\pi m_y = \chi_{yx} \frac{\partial \Psi}{\partial x} + \chi_{yy} \frac{\partial \Psi}{\partial y}$$

From Maxwell's equation $\nabla \cdot \bar{b} = \nabla \cdot (\bar{h} + 4\pi\bar{m})$ we obtain

$$\nabla^2\Psi + 4\pi\nabla \cdot \bar{m} = 0 \tag{2.22}$$

Combining the last two equations, and keeping in mind that $\chi_{xy} = -\chi_{yx}$, the equation for the scaler magnetic potential is found:

$$(1 + \chi_{xx})\left(\frac{\partial^2}{\partial x^2} + \frac{\partial^2}{\partial y^2}\right)\Psi + \frac{\partial^2\Psi}{\partial z^2} = 0. \tag{2.23}$$

This is known as Walker's equation. Outside the sample, Laplace's equation holds:

$$\left(\frac{\partial^2}{\partial x^2} + \frac{\partial^2}{\partial y^2} + \frac{\partial^2}{\partial z^2}\right)\Psi = 0 \tag{2.24}$$

It should be pointed out that (2.23) reduces to (2.24) when χ_{xx} is zero.

Boundary conditions require that Ψ and the normal component of $(\nabla\Psi + 4\pi\bar{m})$ be continuous at the boundary of the spheroid; furthermore, Ψ must approach zero at large distances. It is convenient to introduce a system of spheroidal coordinates defined by[13,17]

$$x = (a^2 - b^2)^{1/2}\,(1 + \xi^2)^{1/2}\,(1 - \eta^2)^{1/2}\cos\phi$$

$$y = (a^2 - b^2)^{1/2}\,(1 + \xi^2)^{1/2}\,(1 - \eta^2)^{1/2}\sin\phi \tag{2.25}$$

$$z = (a - b)^{1/2}\xi\eta$$

in terms of which the surface of the spheroid, $(x^2 + y^2)/a^2 + (z^2 / b^2) = 1$, is given by

$$\xi = \xi_0 = \sqrt{b^2/(a^2 - b^2)} = \sqrt{a^2/(1 - \alpha^2)}, \tag{2.26}$$

where $\alpha = b/a$.

The solution of (2.21) has the form

$$\Psi = Q_n^m (i\xi) P_n^m (\eta) e^{im\phi}, \tag{2.27}$$

where P_n^m and Q_n^m are associated Legendre functions of the first and second kind. The index n is a measure of the periodicity in the polar angle, indicating sectors of reversal of the r.f. magnetization along the z-direction. Similarly, the index m is a measure of the periodicity in the azimuthal coordinate, indicating sectors of reversal of the r.f. magnetization in the x-y plane.

The solution of (2.20) is somewhat more complicated,[13] but the result is a finite polynomial in x, y, and z. Matching the solutions of (2.20) and (2.21) at the boundary yields a characteristic equation[13]

$$m\chi_{xy}\alpha^2 = \xi_0 \frac{\partial}{\partial i\xi_0} \log Q_n^m (i\xi_0) - \bar{\xi}_0 \frac{\partial}{\partial i\bar{\xi}_0} \log P_n^m (i\bar{\xi}_0) \tag{2.28}$$

where

$$\bar{\xi}_0^2 = \frac{(1 + \chi_{xx})\alpha^2}{1 - (1 + \chi_{xx})\alpha^2} \tag{2.29}$$

For a sphere, where a = b, (2.28) reduces to

$$n + 1 + im\chi_{xy} + S \frac{d}{dS} \log P_n^m (S) = 0, \tag{2.30}$$

where

$$S^2 = 1 + 1/\chi_{xx}. \tag{2.31}$$

Equation (2.28) has $1 + \frac{1}{2}(n - |m|)$ roots.[5] Hence, the magnetostatic modes of a spheroid can be labeled (n,m,r), where $r + 1$ is the order of the root of (2.28). The modes so classified are called Walker modes.

Of particular relevance to the experiments dealt with by this thesis is the treatment of magnetostatic modes of a normally-magnetized infinite slab by Damon and van de Vaart.[18] The derivation of the characteristic equation for the slab is similar to the derivation of (2.25) for the spheroid. Equations (2.23) and (2.24) are solved in cylindrical coordinates under identical boundary conditions. An unfortunate difference exists between the theoretical assumptions of the analysis of the normally-magnetized slab and the experimental conditions encountered in the present work, that being the assumption that the hypothetical slab had a uniform internal field described by $H_i = H - 4\pi M$.

In the experiments, a significant feature of the sample was its non-uniform internal field configuration. Damon and van de Vaart did proceed in their analysis by considering the non-uniform demagnetizing factor for a disk. Due to its axial symmetry, however, the magnetostatic mode spectrum for a disk is presumably much less complicated than that for a rectangular slab of the type used in the experiments.

SECTION 3.0

Magnetic Steering of Magnetostatic Bulk Waves

Using the background theory presented in the first two sections, this section will show the dependence of the beam steering angle (the angle between the direction of power flow and the k-vector) on the magnetic field angle (the angle between the magnetic field inside the ferrite medium and the k-vector). The sensitivity of this dependence will be emphasized, and possible device applications suggested. This section follows closely a discussion in reference (22).

3.1 Theory of Beam Steering

In deriving the relation between the beam steering angle β and the magnetic field angle Ψ, it is first necessary to derive an expression for the Poynting vector, $\bar{P} = \frac{1}{2}\,\bar{e} \times \bar{h}^*$, where $\bar{e}$ and $\bar{h}$ are derived from Maxwell's equations. The average power flow per unit area is then $\bar{P}_{av} = \frac{1}{2}\,\mathrm{Re}(\bar{e} \times \bar{h}^*)$. Dividing the magnitude of the cross-product of $\bar{k}$ and $\bar{P}_{av}$ by the dot-product of $\bar{k}$ and $\bar{P}_{av}$ leads to an expression for tan β, where β is the angle between $\bar{k}$ and $\bar{P}_{av}$ (the beam steering angle). The value of tan β will depend on the angle of the wave vector with respect to the magnetic field (the magnetic field angle, Ψ). Upon correcting for the demagnetizing fields within the sample, the desired expression relating the beam steering

angle to the internal magnetic field angle is obtained.

Starting from equation (2.11), which was derived from Maxwell's equations, and substituting

$$\bar{\bar{\mu}} \cdot \bar{h} = \mu_o (\bar{h} + \bar{m}), \tag{3.1}$$

we obtain

$$k^2\bar{h} - \bar{k}(\bar{k} \cdot \bar{h}) = k_o^2(\bar{h} + \bar{m}), \tag{3.2}$$

where $k_o^2 = \omega^2\varepsilon\mu_o$. To arrive at an expression for $\bar{h}$, we should recognize the fact that

$$\bar{k} \cdot \bar{h} = -\bar{k} \cdot \bar{m} \tag{3.3}$$

This can be inferred from Maxwell's equation

$$\nabla \cdot \bar{b} = \nabla \cdot (\bar{h} + \bar{m}) = 0 \tag{3.4}$$

and the assumed $e^{-j\bar{k} \cdot \bar{r}}$ dependence of $\bar{h}$ and $\bar{m}$. Substituting (3.3) into (3.2) and solving for $\bar{h}$, we obtain

$$\bar{h} = \frac{-\bar{k}(\bar{k} \cdot \bar{m}) + k_o^2\bar{m}}{k^2 - k_o^2} \tag{3.5}$$

Next, using

$$\nabla \times \bar{h} = j\omega\varepsilon\bar{e} \tag{2.22}$$

and solving for $\bar{e}$, assuming $e^{-j\bar{k} \cdot \bar{r}}$ dependence of $\bar{h}$, we obtain

$$\bar{e} = \frac{-\bar{k} \times \bar{h}}{\omega\varepsilon} \tag{3.6}$$

Substituting (3.5) into (3.6) gives

$$\bar{e} = \frac{-k_o^2}{\omega\varepsilon}\frac{\bar{k}\times\bar{m}}{k^2 - k_o^2} = \frac{-\omega\mu_o}{k^2 - k_o^2}(\bar{k}\times\bar{m}) \quad . \tag{3.7}$$

The Poynting vector is then

$$\underline{\bar{P}} = \frac{1}{2}\bar{e}\times\underline{\bar{h}}^* = -\frac{\omega\mu_o}{2(k^2 - k_o^2)}\{(\bar{k}\times\underline{\bar{m}})\times[-\bar{k}(\underline{\bar{m}}^*\cdot\bar{k}) + k_o^2\,\underline{\bar{m}}^*]\} \tag{3.8}$$

where $\underline{\bar{m}}$ is a complex vector.

The beam steering relation is then found by calculating

$$\tan\beta = \frac{|\bar{k}\times\bar{P}_{av}|}{\bar{k}\cdot\bar{P}_{av}} \tag{3.9}$$

The result is

$$\tan\beta = \frac{(k^2 - k_o^2)\sin\Psi\cos\Psi}{k_o^2\left(\frac{m_x^2}{m_y^2} + \cos^2\Psi\right)} \tag{3.10}$$

For very small Ψ and for $k^2 >> k_o^2$, this reduces to

$$\tan\beta \approx \frac{k^2\Psi}{k_o^2\left(\frac{m_x^2}{m_y^2} + 1\right)} \tag{3.11}$$

Assuming circular polarization, $m_x = m_y$, so that (3.11) further simplifies to

$$\tan\beta \approx \frac{k^2}{k_o^2}\frac{\Psi}{2} \tag{3.12}$$

This expression shows that for a wave with wave vector $\bar{k}$

making an angle Ψ with the internal magnetic field, the direction of power flow and hence the group velocity $\bar{v}_g$ is inclined at an angle $\beta + \Psi$. This situation is depicted in Fig. 3.1.

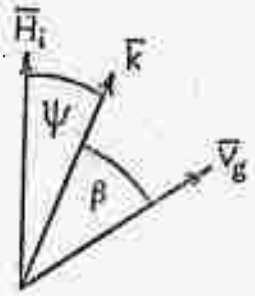

Fig. 3.1 Beam steering angles.

Due to demagnetizing fields, the internal magnetic field angle Ψ will not be equal to the external field angle, which we will call Θ. (see Fig. 3.2). Following (1.18), it is possible to

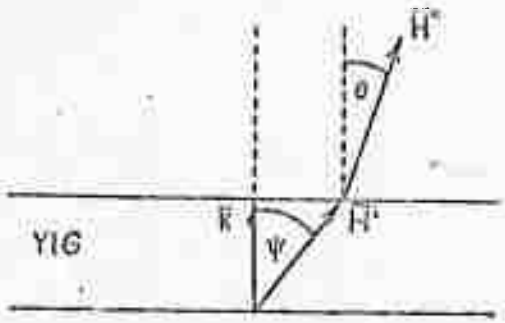

Fig. 3.2 Relationship between internal and external magnetic field angles for a normally-magnetized infinite slab.

express the components of the internal field as

$$H_t^i = H_t^o - N_t \, 4\pi M_s \sin \Psi \tag{3.13}$$

and

$$H_n^i = H_n^o - N_n \, 4\pi M_s \cos \Psi \tag{3.14}$$

for a sample in magnetic saturation, where the superscripts o and i denote external and internal fields, and the subscripts n and t denote normal and transverse quantities. Assuming the sample to be an infinite slab, the normal component of the demagnetizing factor is unity, and the transverse component is zero. Equations (3.13) and (3.14) then become

$$H^i \sin \Psi = H^o \sin \Theta \tag{3.15}$$

and

$$H^i \cos \Psi = H^o \cos \Theta - 4\pi M_s \cos \Psi, \tag{3.16}$$

where the components of the field quantities have been expressed in terms of the angles Θ and Ψ. The ratio of (3.15) and (3.16) gives

$$\tan \Psi = \frac{H^o \sin \Theta}{H^o \cos \Theta - 4\pi M_s \cos \Psi} \tag{3.17}$$

which, for small Ψ, can be written

$$\Psi \simeq \frac{H^o \Theta}{H^o - 4\pi M_s} \tag{3.18}$$

Substituting this into (3.12) gives the expression relating the beam steering angle β to the external magnetic field angle Θ:

$$\tan \beta = \frac{k^2}{k_o^2} \frac{1}{2} \left(\frac{H_o \Theta}{H_o - 4\pi M_s} \right) \tag{3.19}$$

If the wave vector $\bar{k}$ is normal to an infinite slab of thickness d, the lateral displacement x of the beam after having been steered through the crystal will be

$$x = d \tan \beta = \frac{k^2}{k_o^2} \frac{d}{2} \left(\frac{H_o \Theta}{H_o - 4\pi M_s} \right) \tag{3.20}$$

To demonstrate the sensitivity of x to small changes in Θ, we will assume $k = 10k_o$ (putting us in the magnetostatic region of the spin-wave spectrum), $H_o = 2780$ oe., $4\pi M_s = 1780$, $d = 2$mm, and $\Theta = .5° \approx .01$ radians. Then, $x = 2.78$mm, corresponding to a beam steering angle of $\beta \approx 54°$.

According to (3.20), the sensitivity will increase without bound as k increases. In arriving at (3.20), however, the effects of exchange have been neglected. As k is increased beyond the magnetostatic range, these effects become important. Intuitively, the slower the group velocity of the wave, the longer it will be in the ferrite medium under the influence of the steering mechanism, and the more it will be steered. The spin-wave dispersion relation (Fig. 2.1) has an inflection point at[19]

$$k_x \approx \lambda^{-1/4} k_o^{1/2} \tag{3.21}$$

corresponding to a group velocity minimum of[19]

$$v_g \approx 4\lambda k_x \omega_m. \tag{3.22}$$

Typically, $k_x \approx 10^3$ cm^{-1} and $v_g \approx 400$cm/s. Had the exchange parameter λ been accounted for in the derivation of the beam steering relation (3.20), the function would have had a maximum approximately given by (3.21).

As k is increased beyond k_x, the spin-wave region of the dispersion relation is entered, and the group velocity increases. It was for magnetoelastic wave propagation, in fact, that the concept of beam steering was first introduced.[20]

3.2 Applications

Brief mention should be made of possible applications of the beam steering principle. A fine wire transducer could be used to excite magnetostatic spin waves in a thin rectangular crystal; by varying the angle of the external magnetic field, the power could be steered through the crystal to any of several similar transducers on the other side. This is a switching application. The angular variation of the magnetic field could be achieved by adding a small transverse field to the existing field. Thus, the switching of the r.f. power would be controlled by the small amount of current necessary to supply the transverse field.

Since the extent of beam steering is dependent on the frequency of excitation, a similar arrangement (with

fixed magnetic field angle) could be used as a multi-channel filter. The various components of a multifrequency input would be sorted out by the beam steering phenomenon, and individually received by transducers properly positioned on the other side of the crystal.

SECTION 4

Experimental Setup and Results; Localized Resonance

In this section are described the experimental procedures used in attempts to observe beam steering in single-crystal yttrium iron garnet. The geometrical arrangement of the YIG sample and the input-output transducers for the beam steering experiment is shown in Fig. 4.1. The displacement x of the output

Fig. 4.1 Geometry of beam steering experiment.

transducer is varied for a fixed value of the external magnetic field angle, θ. The beam steering theory predicts that a maximum signal will be detected for the value of x given by (3.20).

The experiments that were performed revealed that the energy path through the crystal was, as expected, not colinear with the externally applied d.c. magnetic field. There were discrepancies between theory and experiment, however, which suggested that another mechanism was primarily responsible for the angular deviation of the energy path. The particular mechanism believed to be responsible for the observations is

discussed, along with possible device applications.

4.1 Circuit Description

The microwave circuit diagram is shown in Fig. 4.2. The signal source is an S-band sweep oscillator (Alfred 650) leveled by a -10db sample of its signal, provided by a directional coupler (Narda 3003-10). A frequency meter (HP 536A), a 0-50db precision attenuator (Alfred E103), and a circulator (Sperry Rand D42S21) are included in the circuit between the sweep oscillator and the YIG crystal. The circulator serves as an isolator for most experiments (in which case a matched load terminates the third junction), although it also finds use when reflected signals are measured. After passing through the sample, the signal is detected using a crystal detector (HP 420A), and then displayed on an oscilloscope (Tektronix 535A). The output of the scope is used to drive the y-axis input of an x-y recorder (Mosley 7030A). The field of the laboratory magnet is controlled with a regulated power supply (Varian Fieldial Mark II), and measured with a gaussmeter (Rawson 944). An output from the gaussmeter and a ramp output from the sweep oscillator are available to drive the x-axis of the recorder. In addition, the ramp output from the oscillator is used to provide a frequency base for the scope in many experiments.

Fig. 4.2 also shows a piece of equipment which is designed to convert mechanical positions of the sample

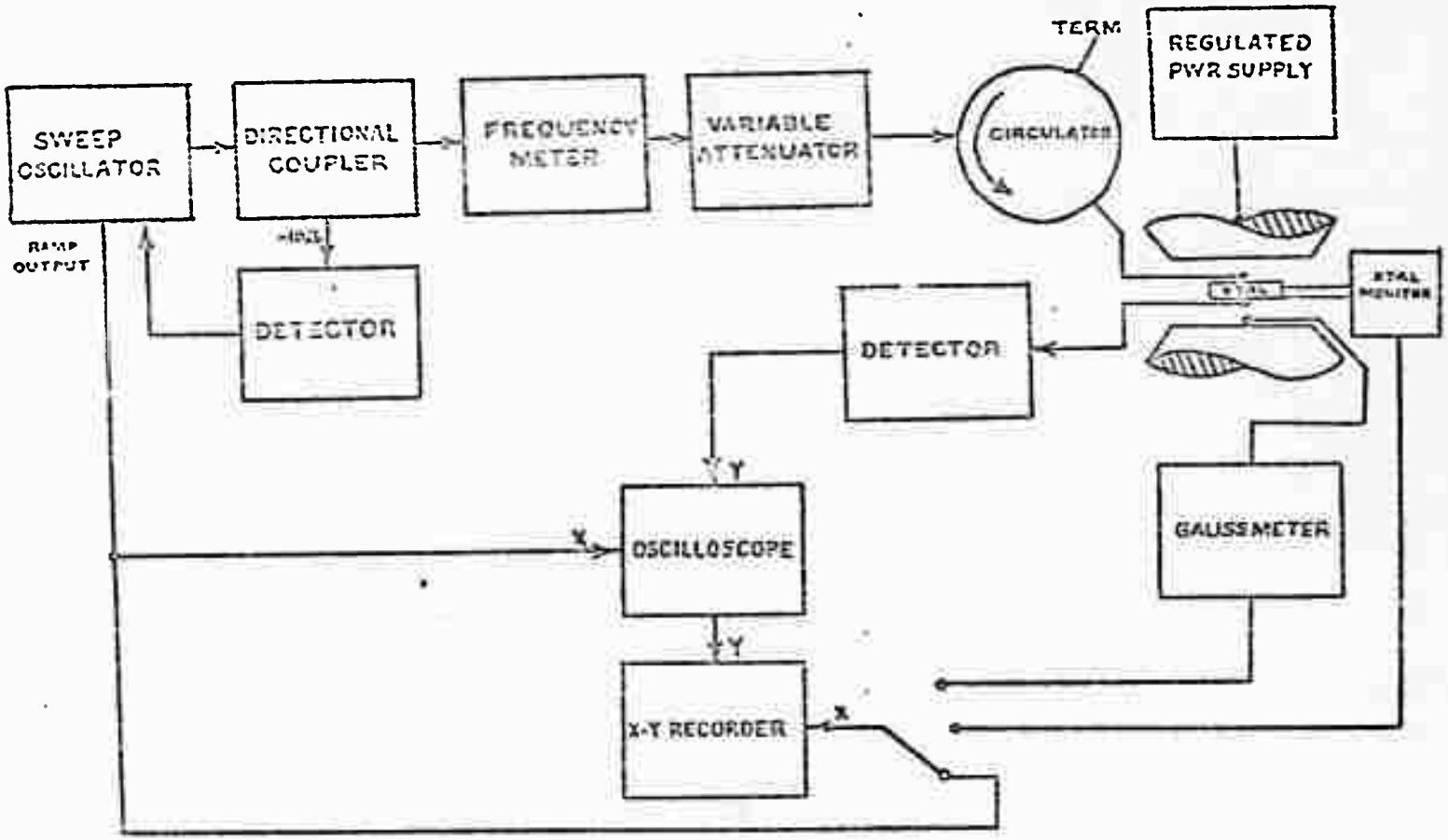

Fig. 4.2 Microwave circuit diagram.

holder to an electrical signal suitable for the x-axis input of the recorder. This, along with the sample holder, will be described shortly in detail.

The single-crystal YIG sample (Airtron) is a thin rectangular slab, measuring .191 × .162 × .018 inches. The slab is cut along the (110) plane, and optically polished. In all experiments, the sample is magnetized nominally in the (110) direction.

4.2 Sample Holder and Associated Equipment

In order to demonstrate beam steering, it was necessary to design a holder for the crystal which would allow for the excitation of waves through the crystal, the detection of these waves, and the measurement of the extent of beam steering. This design was complicated by the fact that the crystal is only .018" thick. Although a thin crystal has the advantage of minimizing the non-uniformity of the internal magnetic fields, there is the disadvantage that the steering effect becomes increasingly hard to measure. In particular, the lateral displacement of a beam steered through the available crystal at an angle of 45° would be only .018".

The geometry of the beam steering problem suggests fine-wire excitation, as opposed, for example, to microwave cavity excitation. The crystal holder, shown approximately full size in the exploded view of Fig. 4.3, consists of two brass blocks which slide together on a

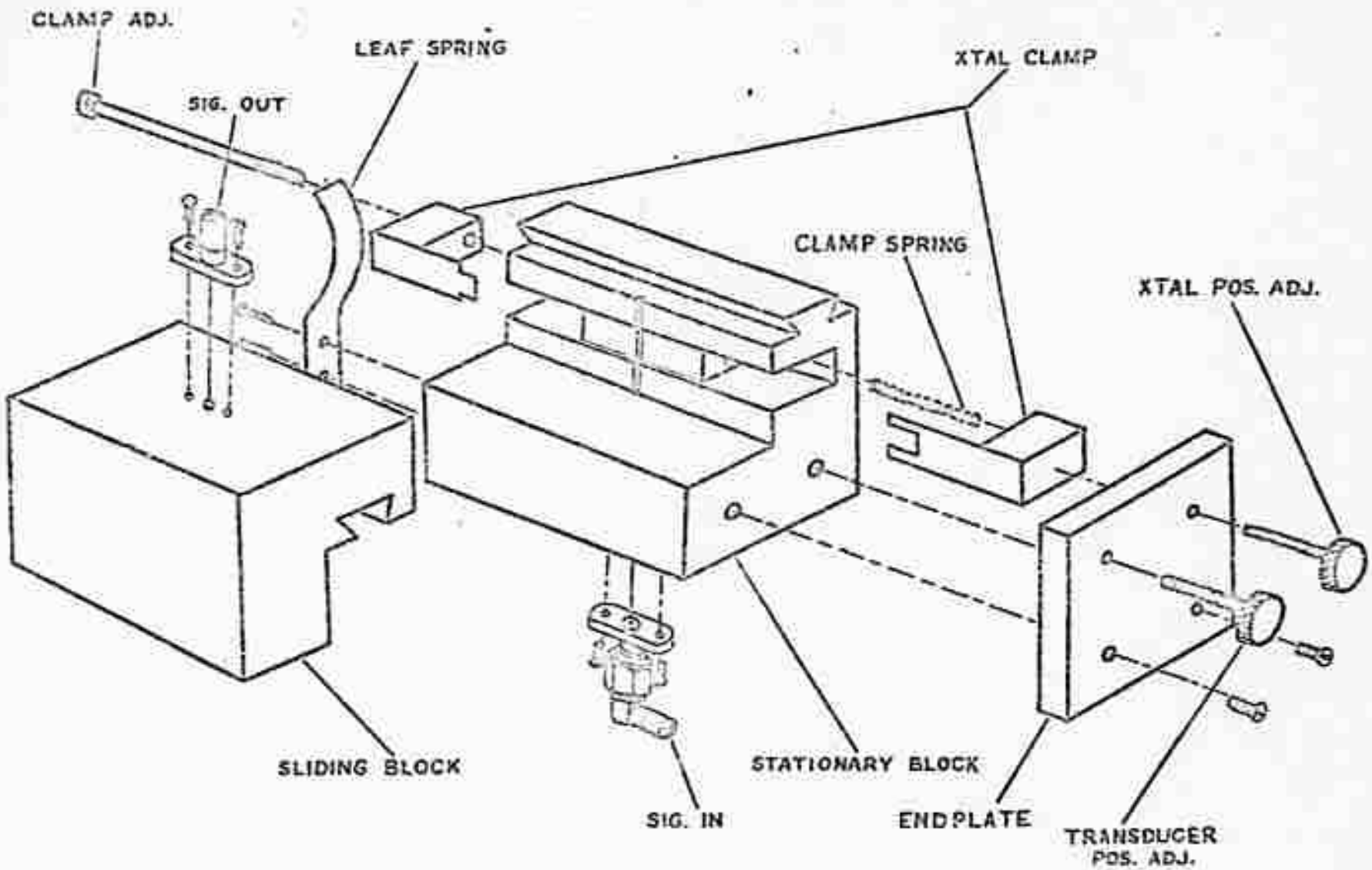

Fig. 4.3 Exploded view of sample holder.

dovetail such that only lateral relative motion is allowed. A narrow groove cut in the sliding surface of each block, perpendicular to the direction of sliding, accomodates the transducer used for the excitation or detection of these waves. These grooves contain narrow teflon inserts which serve to isolate the transducers from the brass, thereby preventing accidental shorts and minimizing capacitive loss.

A coaxial OSM connector mounted on each block provides access to the transducer in that block. Each enamel-insulated fine-wire (.005" dia.) transducer is soldered at one end to the center conductor of its connector. The wires are seated in a fine slot cut in each teflon insert, and each wire is grounded at the other end to its block. Originally, a shallow rectangular recess routed in the sliding surface of the stationary block supported the crystal in its proper position between the two transducers; later, it became necessary to modify the sample holder in order to allow the position of the crystal to be varied while a fixed (usually zero) lateral displacement was maintained between the transducers. Fig. 4.3 shows the sample holder after this modification was made. This feature will be discussed later in this chapter; suffice it to say for the present that this change would have had no effect on the early beam steering experiments.

The sliding block is held firmly against a micrometer-

type thumbscrew (40 threads per inch) by a leaf spring. (The leaf spring is mounted on the stationary block, and must be removed if the blocks are to slide complete apart.) The thumbscrew advances through a tapped hole in a plate which is mounted on one end of the stationary block. The desired lateral displacement between the two transducers is obtained by turning this screw. This provides for the measurement of beam steering.

The photographs of Fig. 4.4 show the sample holder on its mounting bracket. When the blocks are together, the crystal and transducers are hidden from view, as in (a). Fig. 4.4 (b) shows the sample holder with the sliding block removed, revealing the YIG crystal, which appears as a dark rectangle in the middle of the holder. The short vertical strips above and below the crystal in (b) are strips of copper used to mask the input transducer so that only that part of the signal which passes through the crystal is seen by the detection transducer. The purpose of the keyed shaft extending to the right in both views will be discussed later.

In the beam steering experiments, the assembly is mounted to an adjustable table (located between the poles of the laboratory magnet) which allows the angle of the crystal with respect to the magnetic field to be varied. The table is graduated in degrees and provided with a vernier scale so that angles can be measured to the nearest tenth of a degree.

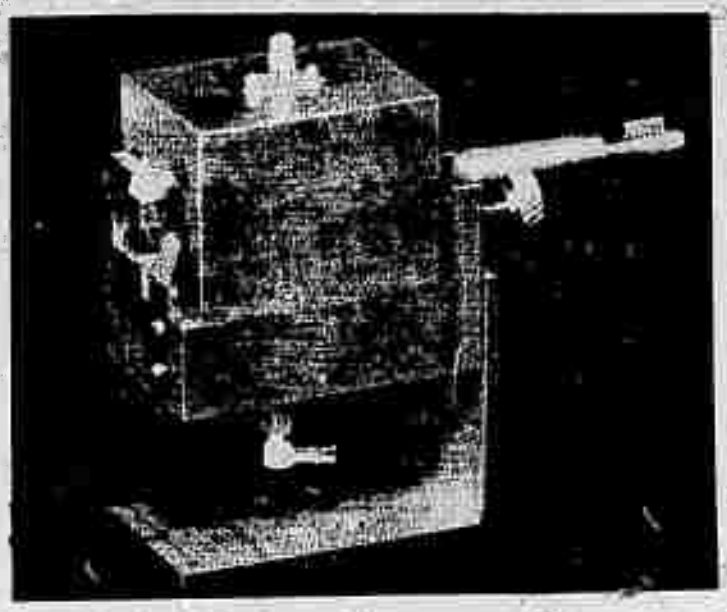

(a)

Reproduced from best available copy.

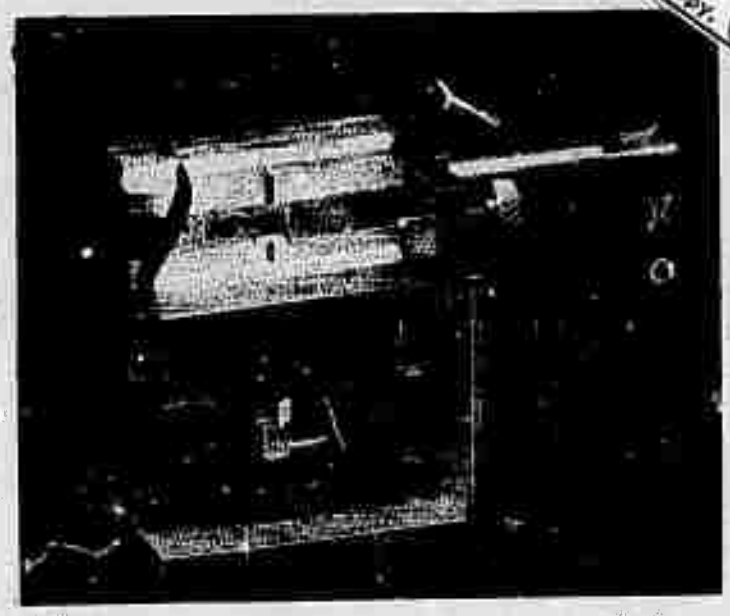

(b)

Fig. 4.4 (a) Photograph of sample holder with mounting bracket, (b) with sliding block removed to reveal YIG sample.

A piece of equipment was designed and built which converts the displacement between the transducers to an electrical signal suitable as an input to the x-y recorder. The device consists of a shaft which is rotated manually, and geared to a ten-turn potentiometer. A counter indicates the number of times the shaft has turned, and a small voltage tapped from the potentiometer gives an electrical output proportional to the angular position of the shaft. A concentric hole drilled into the end of the shaft which extends between the poles of the magnet† is furnished with a keyway. This allows the shaft to slip over the keyed shaft extending to the right in Fig. 4.4. The keyed shaft is threaded at the other end, and may be used in place of either thumbscrew shown in Fig. 4.3. A collar mounted to the endplate of the sample holder surrounds the keyed shaft to prevent it from binding at the threaded end.

The experimental setup is shown in Fig. 4.5. The long shaft extends from the black box to the sample holder, located between the poles of the magnet (a crystal detector is shown mounted directly to the top of the sample holder). Turning the counter dial shown in the foreground rotates the long shaft, which forces the keyed shaft to rotate, while allowing it to advance through the tapped hole in the

---

† The shaft is made of non-magnetic stainless steel so as not to perturb the field pattern inside the magnet.

Reproduced from best available copy.

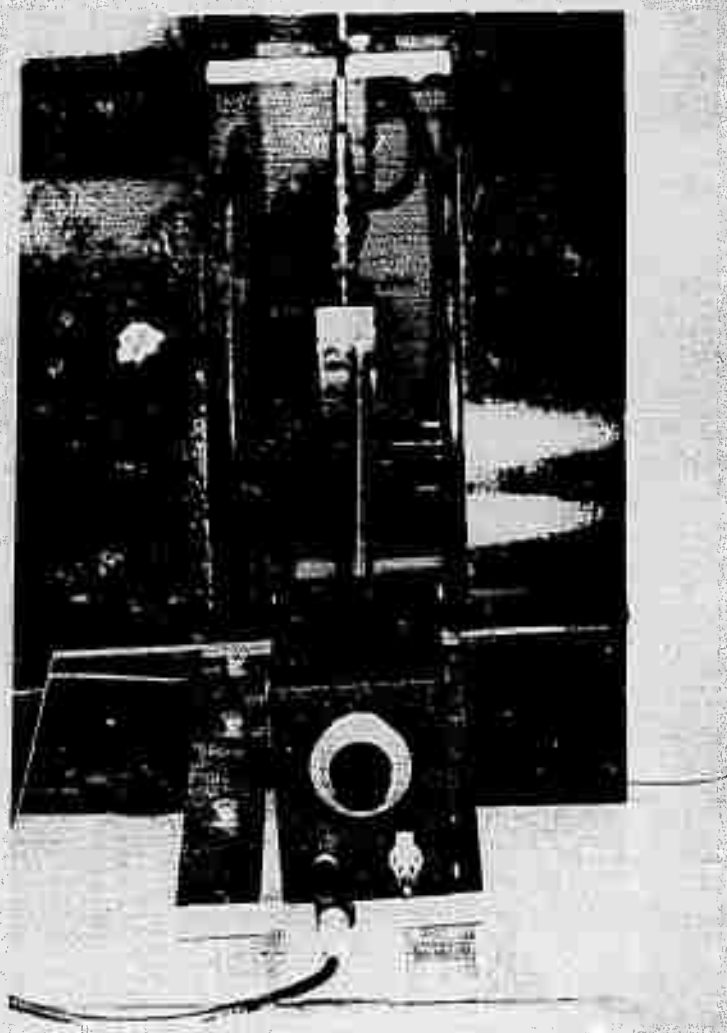

Fig. 4.5 Experimental arrangement for monitoring transducer displacement or crystal position.

endplate. Depending on the experimental arrangement, this will change either the displacement between the transducers or the displacement of the crystal. (In either case, a full ten turns corresponds to a displacement of 1/4", which is slightly more than the length of the crystal.) A visual indication of the displacement is given by the counter, and a voltage proportional to the displacement is available for the x-axis of the recorder.

4.3 Description of Experiments

In the first of a series of experiments directed toward the observation of beam steering, a 1 GHz signal modulated by 1 μs pulse was used to excite the crystal. The equipment required for this experiment is not all shown in Fig. 4.2. The additional equipment included a PIN modulator (HP 8732B), a pulse generator (HP 8403A), a transistor r.f. amplifier (Avantek AWM - 4050M/PS-5), a tunnel diode (Aertech D 112B) in place of the crystal detector, and a pulse amplifier (HP 462A). The goal of this experiment was to observe the time delay between the leakage pulse traveling at the free-space group velocity associated with spin waves. These experiments did not lead to much success, and it was concluded that the pulse width necessary to observe such a time delay was significantly smaller than what the available equipment could provide.

The continuous-wave experiments were more successful.

A series of magnetostatic modes was excited in the YIG crystal by sweeping the frequency of the r.f. field from 2 GHz to 3 GHz. The displacement between the fine-wire transducers and the angle of the magnetic field were maintained at zero. The external magnetic field strength was 2140 oersteds. Using the output from the scope to drive the y-axis of the recorder and the ramp output from the sweep oscillator to drive the x-axis, the transmission of the crystal was plotted; the series of resonances is shown in Fig. 4.6, superimposed on a scale of untuned insertion loss.

In a similar experiment, the magnetic field strength was swept while the frequency of the r.f. field was kept at 2.6 GHz. The output from the gaussmeter was used to drive the x-axis of the recorder. The series of modes thus obtained is shown in Fig. 4.7. An additional resonance peak not shown in Fig. 4.7 occurred at about 2230 oe. This peak had an amplitude comparable to the peak at 2096 oe.

In a first attempt to actually steer the flow of power, the reception of the transmitted signal was investigated as a function of the position of the detection transducer along the crystal. The r.f. frequency and the magnetic field strength were held constant. The results of this experiment are shown in Fig. 4.8, where the signal strength is plotted as a function of the angular

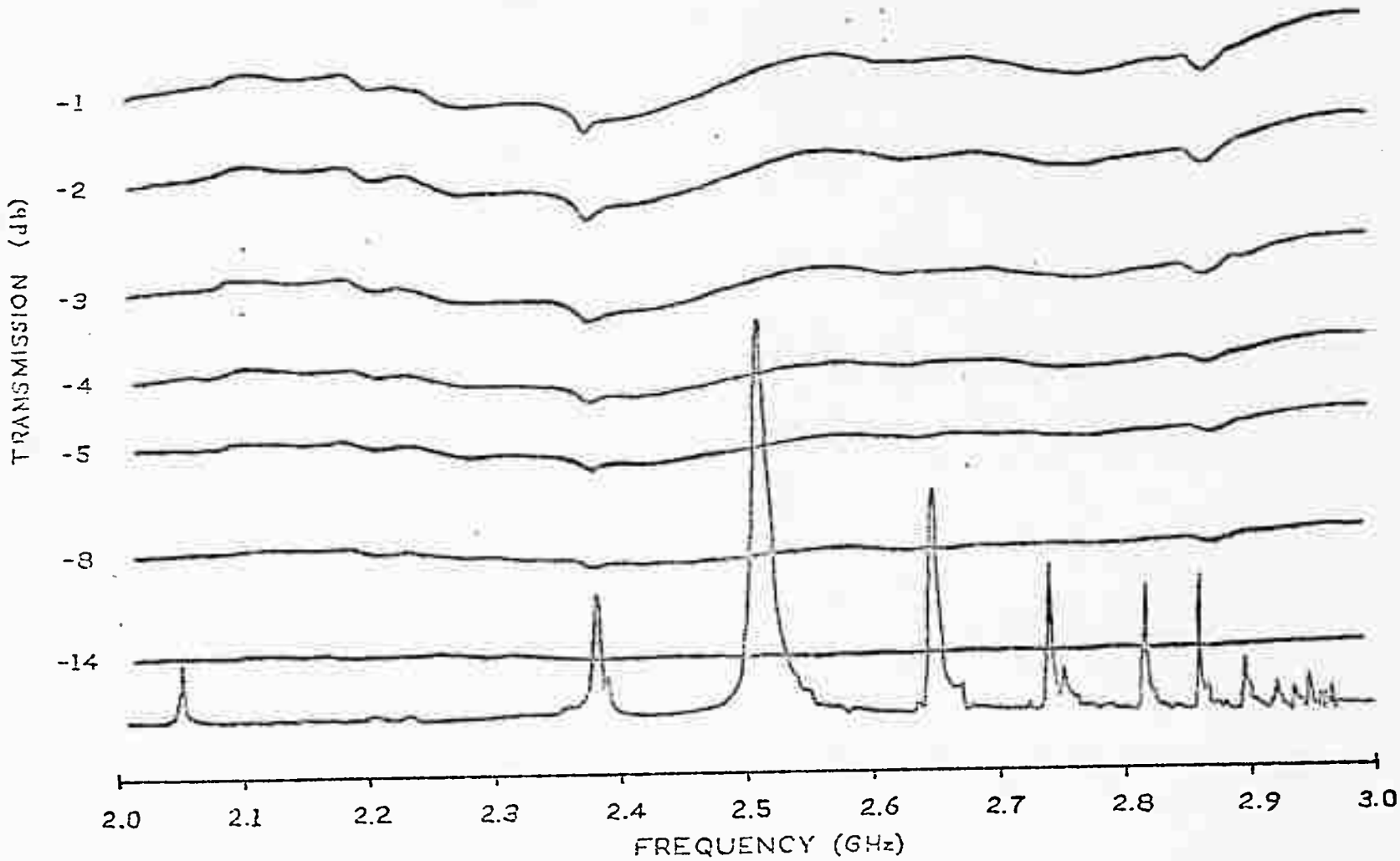

Fig. 4.6 Frequency response of crystal at H_o = 2140 oe.

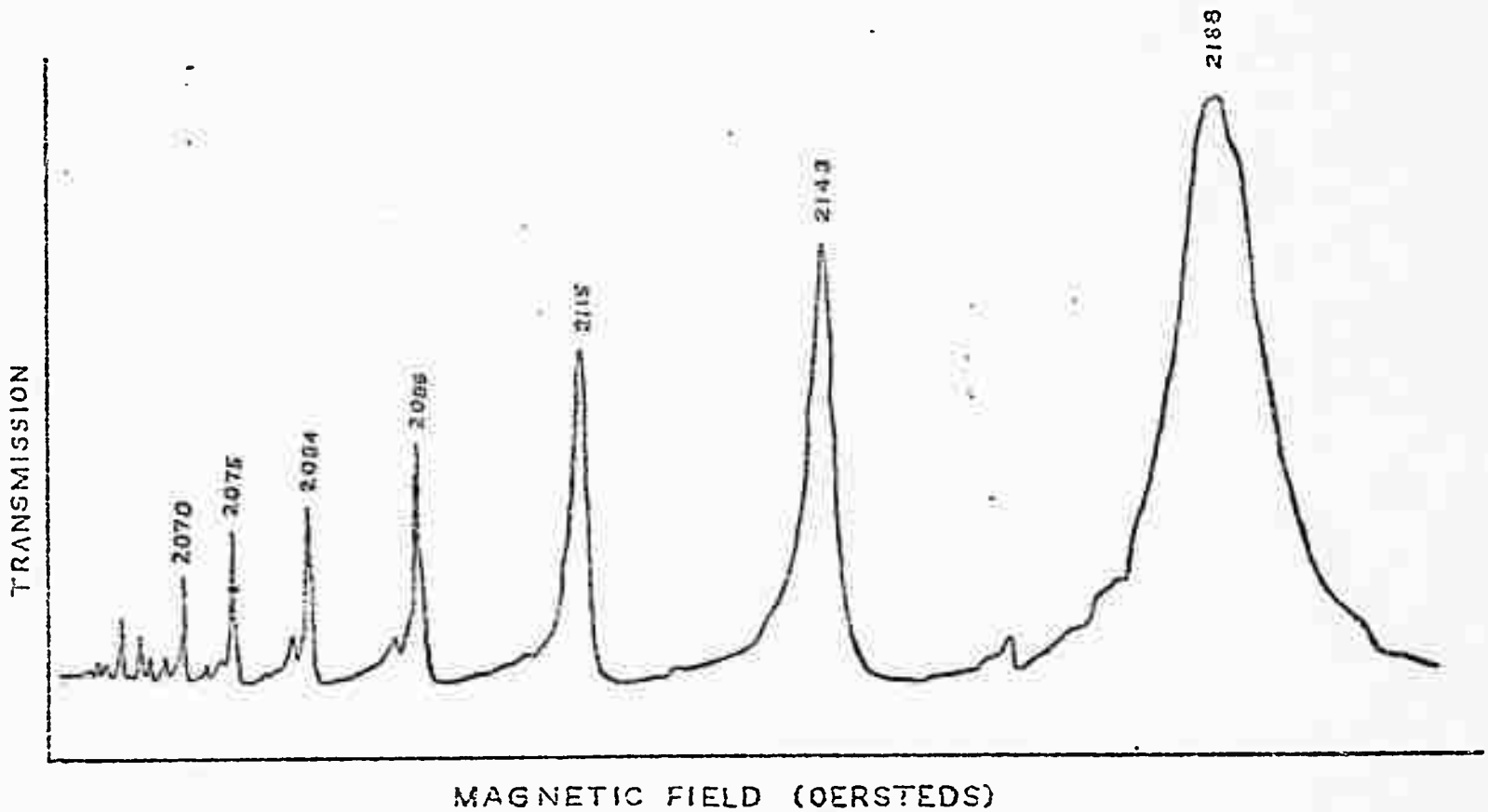

Fig. 4.7 Series of magnetostatic modes excited in YIG sample at f = 2.6 GHz.

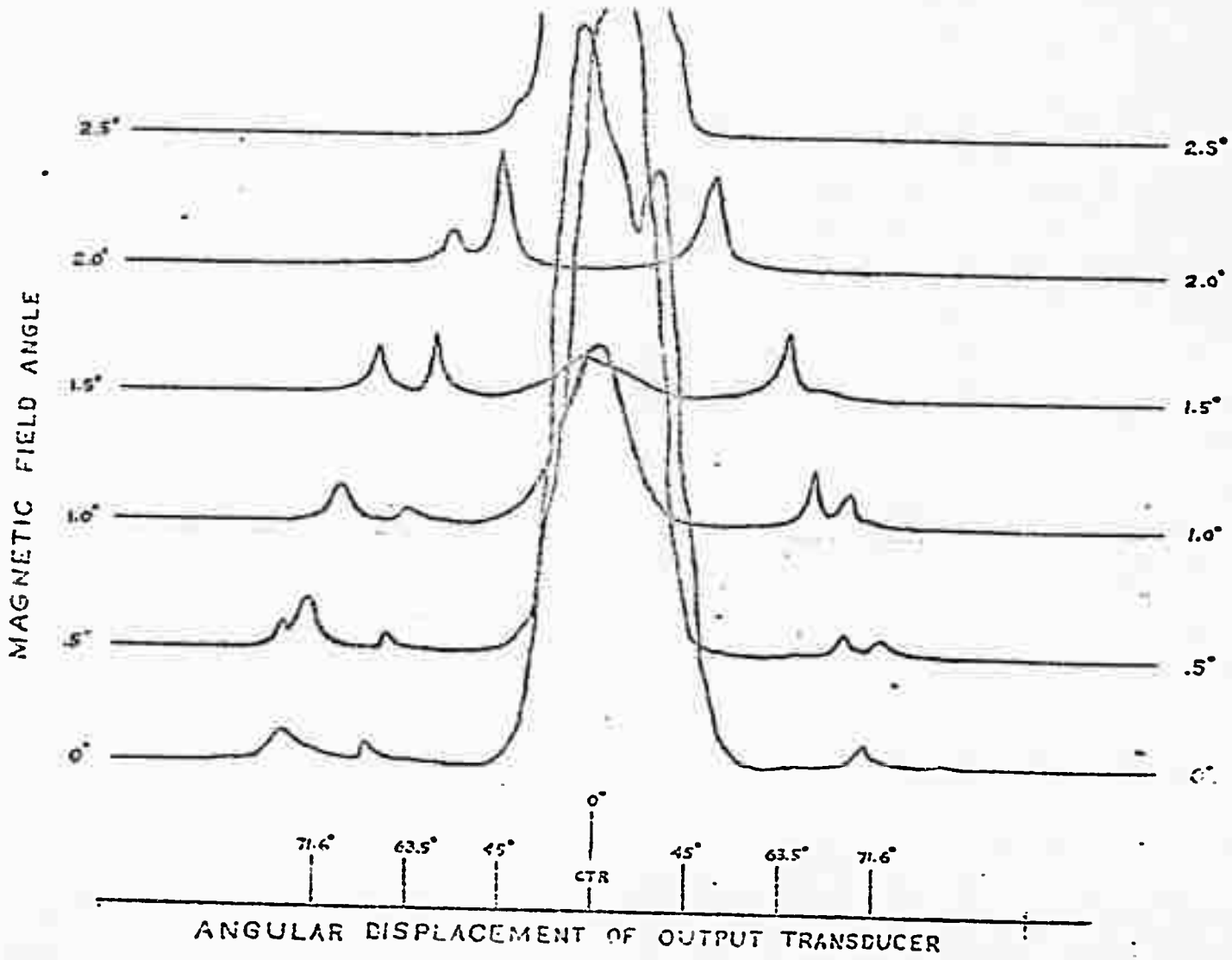

Fig. 4.8 Reception of transmitted signal as a function of the angular displacement of the detection transducer for several values of external magnetic field angle; f = 3.0 GHz, H = 2295 oe.

displacement of the detection transducer for several values of magnetic field angle. This experiment revealed that spatially localized resonances occurred in the crystal. Although it was tempting to interpret this as beam steering, certain qualitative features of the experimental results were inconsistent with the theory. One inconsistent fact was that the localized resonances were symmetrical about the transducer used to excite them. Furthermore, although the external magnetic field angle had an effect on the location of the resonances, a similar effect could be achieved by keeping the magnetic field angle at zero, and varying the strength of the magnetic field.

As was discussed previously, the internal magnetic field in a finite sample is not uniform throughout, but is smaller in the middle of the sample, due to the nature of the demagnetizing field. It was hypothesized that this variation could account for the localized resonances which were observed in the crystal.

To check whether this was indeed the case, a modification was made on the sample holder. This modification allowed the position of the crystal to be varied while a zero lateral displacement was maintained between the transducers. Fig. 4.3 shows how this is done. A coiled wire spring in the stationary block forces one half of a clamping device against a thumbscrew which can advance

through a tapped hole in the endplate. The two components of the clamp are drawn together by a long screw which passes through a clearance hole in the large stationary block and through the coiled wire spring. The crystal nests between the mortise and tenon of the clamp, as shown in Fig. 4.4 (b). The assembly is free to move horizontally approximately 1/4" in either direction. This motion is accomplished by rotating the thumbscrew, or, for the experimental arrangement shown in Fig. 4.5, by turning the counter dial.

With this new feature, it was possible to plot a "transmission profile" of the crystal; i.e., the transmission of the crystal as a function of its position between the transducers. This experiment was performed at an excitation frequency of 2.68 GHz for several values of magnetic field strength; the magnetic field angle and the lateral displacement between the transducers were fixed at zero. The results are shown in Fig. 4.9, where the word "displacement" labeling the x-axis refers to the nominal distance between the vertical axis of symmetry of the crystal and the transducers.

In a similar experiment, the magnetic field strength was held constant at 2170 oe., and a transmission profile was plotted for several excitation frequencies. The results are shown in Fig. 4.10. The magnetic field strength and increments of frequency were chosen such that the curves would resemble those in Fig. 4.9.

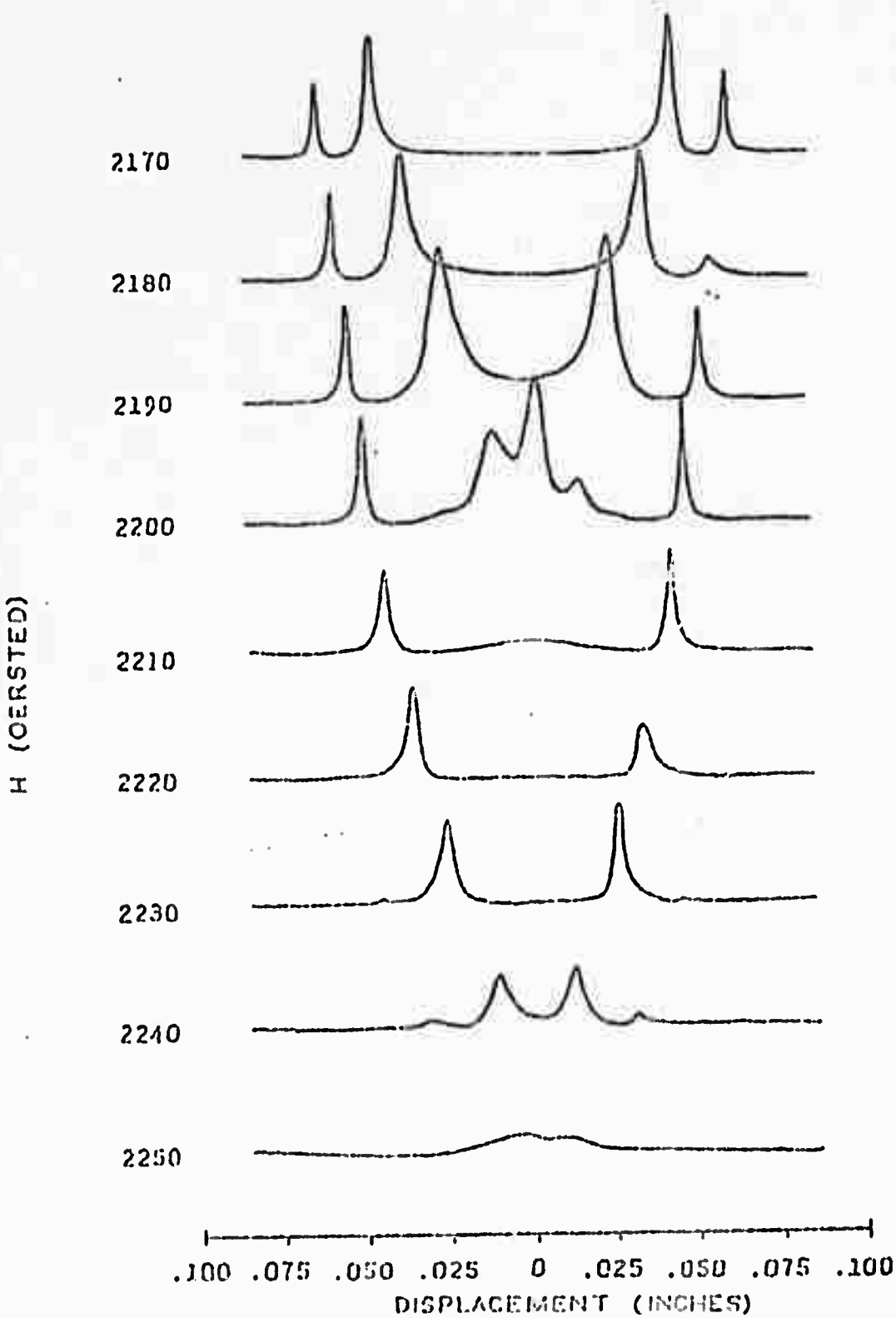

Fig. 4.9 Transmission profile of crystal for various values of magnetic field for f = 2.68 GHz.

The inverse of this latter experiment was also performed; that is, the frequency response of the crystal was plotted while the displacement was varied as a parameter, with the magnetic field strength held constant at 2210 oe. Fig. 4.11 shows how the frequency response of the crystal depends on its position between the transducers. Note that the local frequency response is shifted upward as the edge of the crystal is approached. Note also that this shift appears to be nonlinear in frequency -- that the resonance of lowest frequency experiences the greatest shift, resulting in a compression of the frequency response.

The appearance of the curves in Fig. 4.9 suggested a final experiment. By increasing the external magnetic field to compensate for the decrease in the internal magnetic field near the center of the crystal, it was possible to track a resonance, corresponding to a single frequency, as the position of the crystal between the transducers was varied. The external field values required to do this are plotted as a function of the displacement of the crystal in Fig. 4.12.

4.4 Interpretation of Results

From the experiments it was concluded that the non-uniformity of the internal magnetic field was responsible for the localized resonances. Non-uniform magnetic fields in crystals are generally undesirable, and in the present work overshadowed the beam steering effect; certain

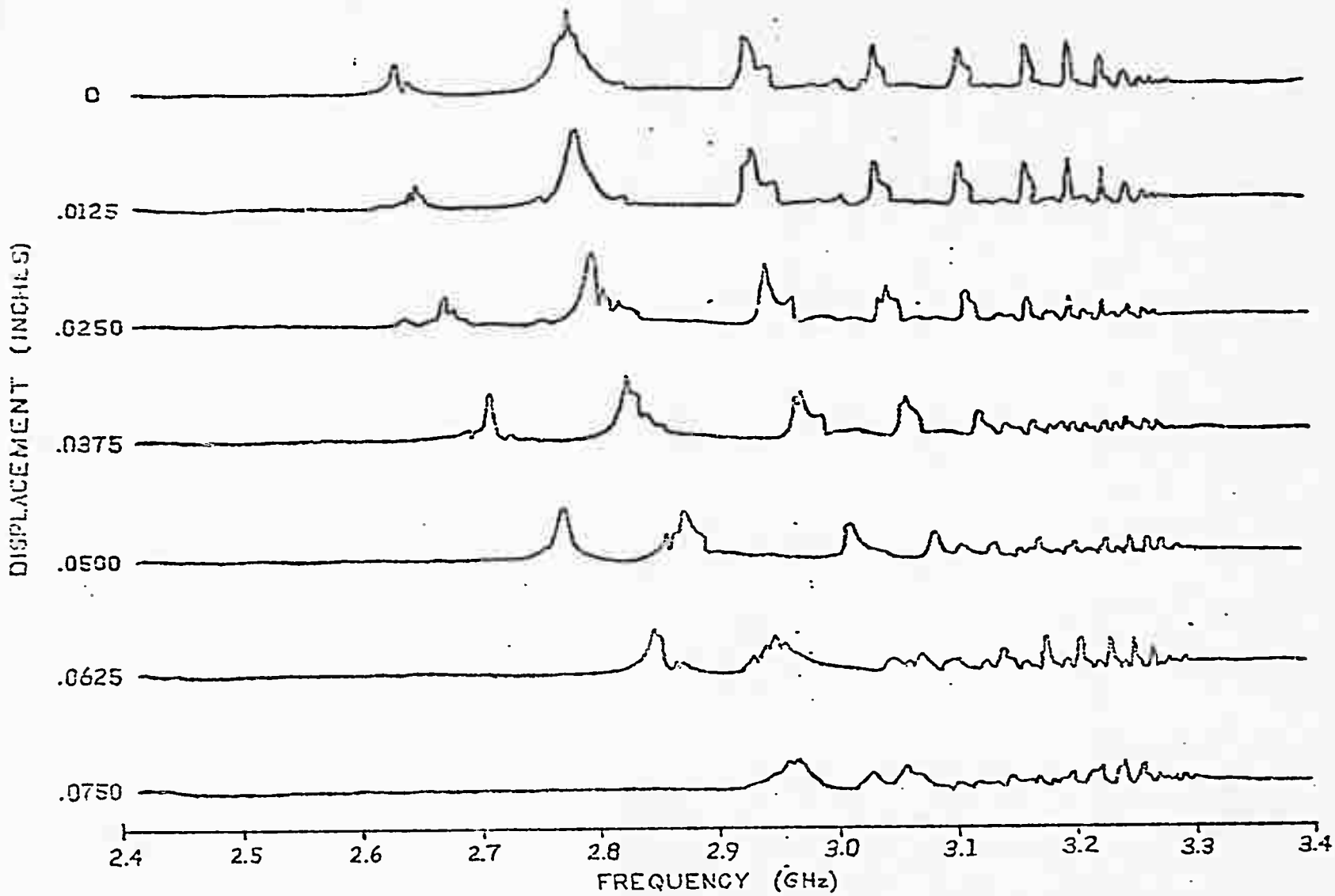

Fig. 4.11 Frequency response of crystal for several values of its displacement for H_o = 2210 oe.

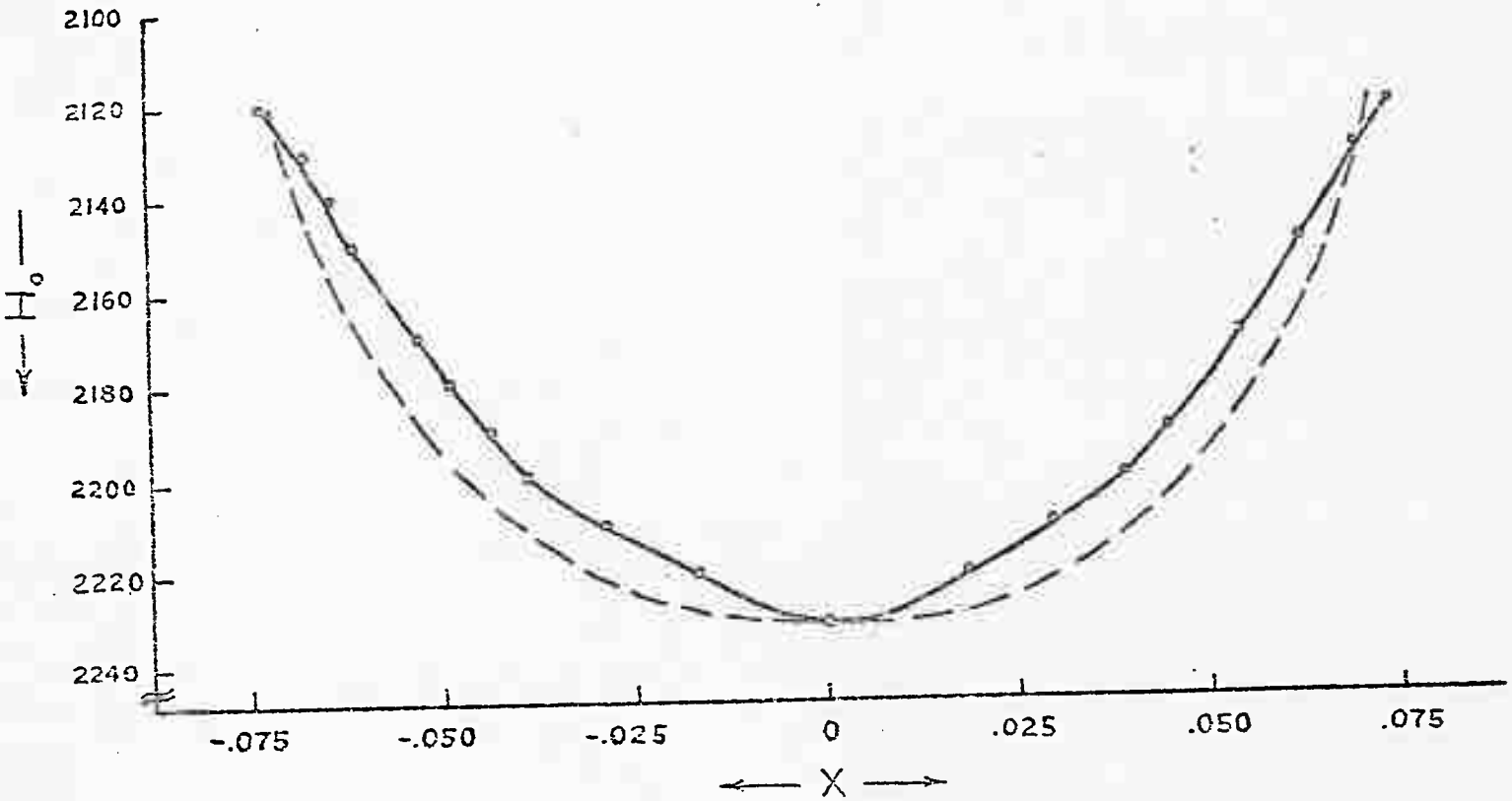

Fig. 4.12 External field required to track a single resonance through the crystal, as a function of crystal displacement: experimental (solid line) and theoretical (broken line).

experimental findings, however, suggest that this non-uniformity might be exploited to some advantage. Before discussing possible applications, it is desirable to have a mathematical model to describe the internal magnetic fields of a rectangular sample. Such a model has been proposed by Joseph and Schlömann,[8] and there have been experimental results which support their model.[21] It has been pointed out that the demagnetizing field is sometimes expressed in terms of a tensorial demagnetization factor N_{ij} by means of the relation (1.19). Joseph and Schlömann have derived the zz component of the demagnetization factor for a rectangular prism with the d.c. magnetic field applied in the z-direction. To first order,

$$N_{zz}(r) = \frac{1}{4\pi}\,[\tan^{-1} f(x,y,z) + \tan^{-1} f(-x,y,z) + \tan^{-1} f(x,-y,z) + \tan^{-1} f(x,y,-z) + \tan^{-1} f(-x,-y,z) + \tan^{-1} f(x,-y,-z) + \tan^{-1} f(-x,y,-z) + \tan^{-1} f(-x,-y,-z)] \quad (4.1)$$

where

$$f(x,y,z) = \frac{(a-x)(b-y)}{[(a-x)^2 + (b-y)^2 + (c-z)^2]^{1/2}(c-z)} \quad (4.2)$$

and where the origin of the coordinate system coincides with the center of the prism and the axes are aligned with the principal axes of the prism. The length of the axes are 2a, 2b, and 2c.

Of particular interest here is the variation of the zz component of the demagnetization factor along the length of the crystal (along x). If this variation is considered to be measured from the middle of the crystal with respect to the other two dimensions, equations (4.1) and (4.2) simplify considerably, since now $f(x,y,z) \rightarrow f(x,o,o)$. Also of interest is the gradient of $N_{zz}\ 4\pi M_s$ (which is equivalent to the gradient of the z-component of the internal magnetic field) with respect to x at $y = z = 0$. Although finding the gradient of (4.1) is somewhat cumbersome, various simplifacations are encountered along the way, with the result that

$$\left.\frac{\partial N_{zz}}{\partial x}\right|_{x,o,o} = \frac{bc}{\pi}\,[g(x,o,o) - g(-x,o,o)], \tag{4.3}$$

where

$$g(x,o,o) = \frac{1}{[(a+x)^2 + c^2][(a+x)^2 + b^2 + c^2]^{1/2}} \tag{4.4}$$

A computer was programmed to calculate $N_{zz}\ (x,o,o)$, $\left.\frac{\partial N_{zz}}{\partial x}\right|_{x,o,o}$, and $\left.\frac{\partial H_i}{\partial x}\right|_{x,o,o}$ $\left(= 4\pi M_s \frac{\partial N_{zz}}{\partial x}\right)$ for the crystal used in the experiments ($a = .0955''$, $b = .081''$, $c = .099''$, $4\pi M_s = 1780$), for values of x ranging from zero to $a = .0955''$, in increments of .0125".† The results are tabulated in Table 4.1. The actual plot of the demagnetizing factor

---

† This increment is the distance a 40 threads per inch screw advances in one-half turn. Mechanical positions of the sample holder were controlled by this type of screw (see Fig. 4.3).

Displacement (inches)	Demagnetizing Factor	$\left.\frac{\partial N_{zz}}{\partial x}\right\|_{x,o,o}$ (inches^{-1})	$\left.\frac{\partial H_i}{\partial x}\right\|_{x,o,o}$ (Oersteds/inch)
0	.9077	0	0
.0125	.9068	.1402	250
.0250	.9040	.3171	564
.0375	.8985	.5897	1050
.0500	.8883	1.0902	1940
.0625	.8688	2.2035	3920
.0750	.8249	5.4666	9720
.0875	.6910	19.5079	34,700
.0955	.4617	35.1209	62,500

Table 4.1 Theoretical values of $N_{zz}(x,o,o)$, $\left.\frac{\partial N_{zz}}{\partial x}\right|_{x,o,o}$, and $\left.\frac{\partial H_i}{\partial x}\right|_{x,o,o}$ for several values of x.

in shown in Fig. 4.13.

In all experiments, the r.f. excitation was localized in x, but distributed over the width of the crystal. Therefore, in proposing a mathematical model to explain the experimental results, it might be more accurate to calculate the theoretical demagnetizing factor averaged over y as a function of x, at z = 0. This average can be written

$$\bar{N}_{zz}(x) = \frac{1}{2b} \int_{-b}^{b} N_{zz}(x,y,o)\,dy$$

$$= \frac{1}{b} \int_{o}^{b} N_{zz}(x,y,o)\,dy, \qquad (4.5)$$

where the bar over $N_{zz}(x)$ denotes an average over y. A computer was programmed to solve (4.5) by a numerical method (the trapezoidal rule), and plot the results. It was found that this refinement in the mathematical model had little effect on the shape of the demagnetizing factor function. The plot of (4.5) is shown together with the plot of $N_{zz}(x,o,o)$ in Fig. 4.13 for comparison.

From the theoretical data given in Table 4.1, it is possible to plot the internal magnetic field of the crystal used in the experiments, as a function of x, given a fixed value of the external field H_o. The expression for this function is

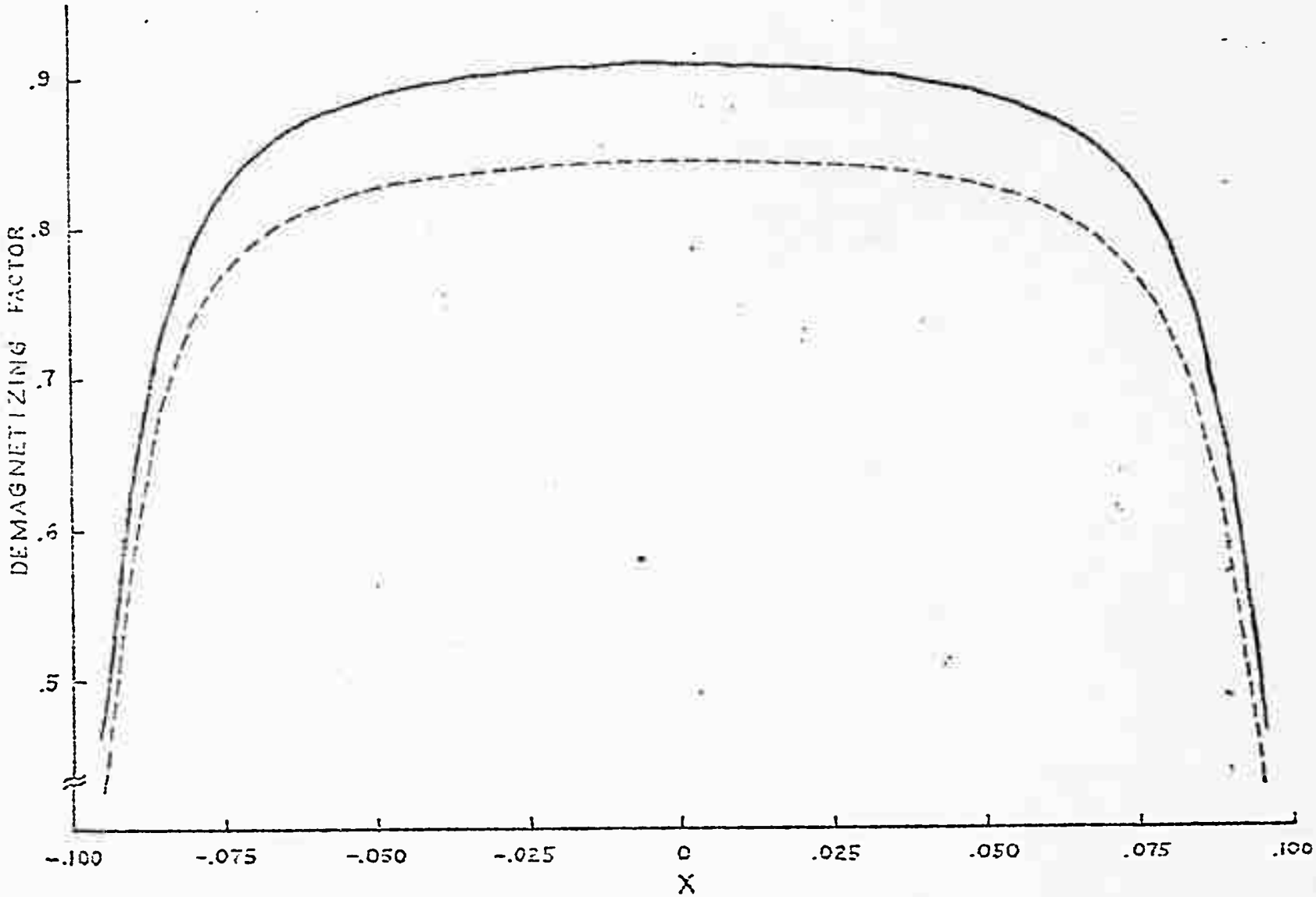

Fig. 4.13 Theoretical demagnetizing factor as a function of position along crystal; for y = 0 (solid line) and averaged over y (broken line)

$$H_i(x) = H_o - N_{zz}(x)\ 4\pi M_s \tag{4.6}$$

where $4\pi M_s$ = 1780 gauss for YIG. It is also possible, however, to plot the theoretical values of external field required to produce a particular internal field at a distance x from the center of the crystal. The resulting plot would be of the function

$$H_o(x) = H_i + N_{zz}(x)\ 4\pi M_s. \tag{4.7}$$

This has been done for H_i = 615 oersteds. The result is shown in Fig. 4.12, together with the experimental plot described in the previous section. The value of H_i = 615 oe. was chosen so that the two plots had the same value at x = 0. The similarity of the plots gives support to the hypothesis that the non-uniform internal magnetic field (due to the spatial dependence of the demagnetizing factor) is at least primarily responsible for the localized resonances. We will proceed by discussing some possible applications.

4.5 Applications

As was seen previously, non-uniform internal magnetic fields in a non-ellipsoidal sample give rise to a spatially-dependent frequency response (see Fig. 4.11). This phenomenon could conceivably be exploited in the design of microwave signal processing devices. A multichannel filter, for example, could be realized by properly locating

three or four fine-wire transducers along one face of the crystal, toward the edge where the internal field gradients are larger. A single fine-wire or narrow-strip transducer on the opposite face of the crystal would allow excitation of the magnetostatic spin waves. The effect that the non-uniform field distribution inside the crystal would have on a multi-frequency input would be to "sort out" the frequencies; the individual frequencies would be available at different positions along the output of the crystal, and would be detected by fine-wire transducers located at these positions. Such a device could be tuned by varying the external d.c. magnetic field. It would have an advantage over, say, a resonant cavity in that only one such device would be required to sort a multi-frequency signal; also, the proposed device would lend itself to stripline technology.

A device which was actually designed along these lines is shown approximately full-size in the photograph of Fig. 4.14. The bottom connector provides access to a narrow strip transducer which allows excitation of the crystal. The top three connectors provide access to fine-wire output transducers. The fine wires are spaced .0125" apart behind the crystal, and separated by a ground plane. This ground plane is necessary to minimize coupling between output ports, which was found to be -27 db maximum

Reproduced from best available copy.

Fig. 4.14 Experimental multichannel filter.

over the S-band frequency range. The close proximity of the fine wires to the ground plane, however, introduces strong capacitive loss. This device is still in the experimental stages; there is presently insufficient data from which to draw conclusions on its performance.

There are some interesting properties of substituted garnets which might be exploited in the design of devices utilizing non-uniform internal magnetic fields. A study by Harrison and Hodges[23] has shown that the saturation magnetization of yttrium aluminum iron garnet is quite dependent on the aluminum content, whereas the linewidth is relatively unaffected by it. Their findings are shown in Fig. 4.15. Although their results were obtained from polycrystals, similar results would be expected for single crystals. If a method could be devised of creating a gradient of aluminum content in the plane of a thin film of yttrium aluminum iron garnet, the film would have a non-uniform saturation magnetization. This would give rise to a non-uniform internal magnetic field, in the same sense that a non-uniform demagnetizing factor is responsible for a non-uniform field inside a thicker sample.

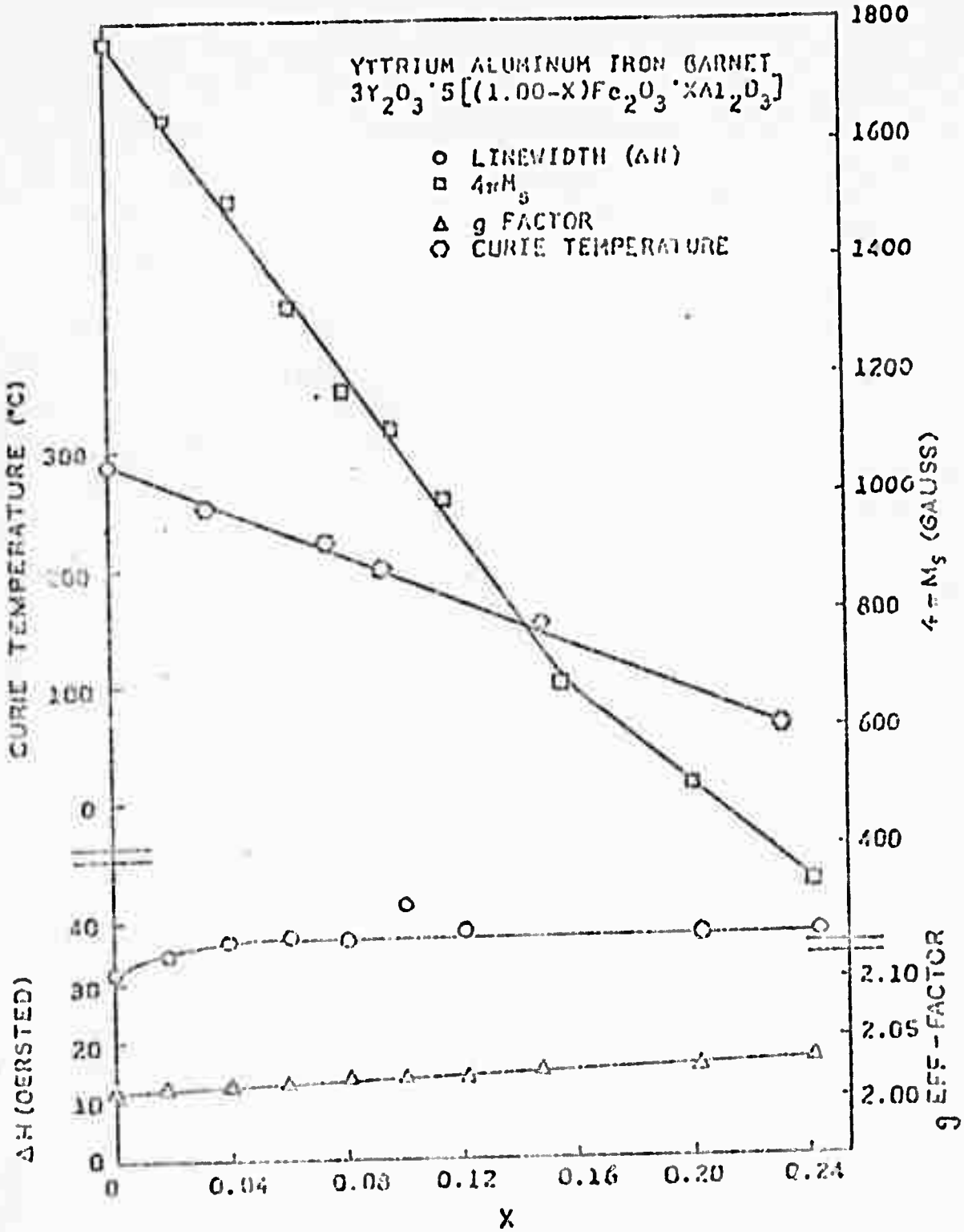

Fig. 4.15 Variation of line width, saturation magnetization, effective g-factor, and Curie temperature with aluminum content in yttrium aluminum iron garnets.[22]

SECTION 5
CONCLUSIONS

As reported in this thesis, the S-band microwave resonances observed in a rectangular slab were characterized by relatively narrow linewidth and low loss. Linewidths of the lower-order modes were approximately 10 oersteds, corresponding to a frequency linewidth of 28 MHz; linewidths as small as one oersted were observed for the lower-order modes. The minimum untuned insertion loss at the largest peak was approximately 3 db. Resonances were observed to be spatially localized to within .0125" near the edge of the crystal, which measured .191" in length. Although this high degree of localization would suggest that the wave number was quite large, the relatively high transmission peaks indicate that the propagation was probably largely electromagnetic in nature.

The beam steering relation, derived for a normally-magnetized infinite slab, revealed that the direction of power flow is very sensitive to the angle between the propagation vector and the d.c. magnetization. However, in our experimental attempts to observe beam steering, we had to contend with a non-uniform internal magnetic field (created by the sample shape) whose effects overshadowed the beam steering that was predicted to occur for slowly propagating spin waves. One method of eliminating this problem would be to make the slab sufficiently thin so that the infinite slab approximation becomes valid, and the

internal field is effectively uniform. Practical considerations place a limit on this solution, since the steering becomes increasingly hard to measure as the thickness of the crystal is reduced. Another solution would be to compensate for the non-uniform demagnetizing factor by placing the sample in an approximately non-uniform external magnetic field, so as to render the internal field uniform.

The occurrence of spatially localized resonances in the experiments was attributed to the large gradients of internal magnetic field encountered in the crystal, particularly near its edge. The values of the external magnetic field necessary to produce a given internal field at different points within the sample was plotted experimentally, and was shown to be in close agreement with theory. It was suggested that the phenomenon of localized resonances might find applications in device technology. Future work along this line might profitably be directed toward the growth of thin films with controlled gradients of saturation magnetization.

References

1. C. P. Slichter, Principles of Magnetic Resonance, with Examples from Solid State Physics, Harper and Row, New York (1963).

2. M. Sparks, Ferromagnetic Relaxation Theory, McGraw-Hill, New York (1964).

3. S. V. Vonsovskii, ed., Ferromagnetic Resonance, Pergamon Press, New York (1966).

4. H. P. J. Wijn, ed., Handbuch der Physik, vol. XVIII/2, Springer-Verlag, Berlin (1966).

5. B. Lax and K. J. Button, Microwave Ferrites and Ferrimagnetics, McGraw-Hill, Inc., New York (1962).

6. C. Kittel, Introduction to Solid State Physics, Wiley and Sons, Inc., New York (1971).

7. S. Chikazumi, Physics of Magnetism, Wiley and Sons, Inc., New York (1964).

8. R. I. Joseph and E. Schlömann, "Demagnetizing Field in Nonellipsoidal Bodies", J. Appl. Phys. 36, 1579 (1965)

9. L. Landau and E. Lifshitz, "On the Theory of the Dispersion of Magnetic Permeability in Ferromagnetic Bodies", Physik Z. Sowjetunion 8, 153 (1935).

10. T. L. Gilbert, A Lagrangian Formulation of the Gyromagnetic Equation of the Magnetization Field", Phys. Rev. 100, 1243 (1955).

11. C. Kittel, "On the Theory of Ferromagnetic Resonance Absorption", Phys. Rev. 73, 155 (1948).

12. J. A. Osborn, "Demagnetizing Factors of the General Ellipsoid", Phys. Rev. 67, 351 (1945).

13. L. R. Walker, "Spin Waves and Other Magnetic Modes", Magnetism, Vol. 1, Rado and Suhl, ed., Academic Press, New York (1963).

14. C. Herring and C. Kittel, "On the Theory of Spin Waves in Ferromagnetic Media", Phys. Rev. 81, 869 (1951).

15. R. L. White and I. H. Solt, Jr., "Multiple Ferromagnetic Resonance in Ferrite Spheres", Phys. Rev. 104, 56 (1956).

16. L. R. Walker, "Magnetostatic Modes in Ferromagnetic Resonance", Phys. Rev. 105, 390 (1957).

17. P. M. Morse and H. Feshbach, Methods of Theoretical Physics, McGraw-Hill, New York (1953).

18. R. W. Damon and H. van de Vaart, "Propagation of Magnetostatic Spin Waves at Microwave Frequencies in a Normally-Magnetized Disk", J. Appl. Phys. 36, 3453 (1965).

19. F. R. Morgenthaler, "Photon/Magnon Conversion Near a Material Interface", Electronics Letters 3, 299 (1967).

20. R. C. Addison, B. A. Auld, and J. H. Collins, "Ray-Theory Analysis of Magnetoelastic Delay Lines", J. Appl. Phys., 39, 1828 (1968).

21. T. Kohane, E. Schlömann, and R. I. Joseph, "Microwave Magnetoelastic Resonances in a Nonuniform Magnetic Field", J. Appl. Phys. 36, 1267 (1965).

22. F. R. Morgenthaler, U.S. Patent Application SN 740, 751 (1968).

23. G. R. Harrison and L. R. Hodges, Jr., "Microwave Properties of Polycrystalline Hybrid Garnets", J. Am. Ceramic Soc. 44, 214 (1961).